






Research Article

Final Amalgamation Processes of the Southern Altaids: Insights from the Triassic Houhongquan Ophiolitic Mélange in the Beishan Orogen (NW China)

Qigui Mao ^{1,2,3,4} Wenjiao Xiao ^{1,3,4,5} Songjian Ao ^{3,4,5} Dongfang Song,^{3,4,5}
Miao Sang,^{1,4} Zhou Tan,^{1,4} Hao Wang ^{1,4} Rui Li ^{1,4} and Meng Wang^{1,4}

¹Xinjiang Research Center for Mineral Resources, Xinjiang Institute of Ecology and Geography, Chinese Academy of Sciences, Urumqi 830011, China

²Redrock Mining. Co., Ltd., Hami 839000, China

³Innovation Academy for Earth Science, CAS, Beijing 100029, China

⁴College of Earth and Planetary Sciences, University of Chinese Academy of Sciences, Beijing 100049, China

⁵State Key Laboratory of Lithospheric Evolution, Institute of Geology and Geophysics, Chinese Academy of Sciences, Beijing 100029, China

Correspondence should be addressed to Qigui Mao; qg-mao@ms.xjb.ac.cn, Wenjiao Xiao; wj-xiao@mail.iggcas.ac.cn, and Rui Li; lirui@ms.xjb.ac.cn

Received 25 September 2022; Revised 27 November 2022; Accepted 4 January 2023; Published 22 February 2023

Academic Editor: Chuan-Lin Zhang

Copyright © 2023 Qigui Mao et al. Exclusive Licensee GeoScienceWorld. Distributed under a Creative Commons Attribution License (CC BY 4.0).

The Permian–Triassic tectonic setting is still controversial in the southern Altaids. The Beishan orogen is an ideal region to address the final tectonic of the Altaids. These systematic mapping, geochemistry, and geochronology studies on the Houhongquan ophiolitic mélange in the south Beishan are conducted to address this issue. New mapping reveals that the Houhongquan ophiolitic mélange consists of blocks of gabbro, basalt, chert, granite, and strongly deformed and cleaved sandstone in the southern Beishan. The studies reveal that the mafic fragments are relics of normal-mid-ocean ridge (N-MOR) and suprasubduction zone (SSZ) types of oceanic lithosphere. The four sandstone matrix samples yield the maximum depositional ages of 222 ± 5 Ma, 233.8 ± 2.3 Ma, 263.4 ± 2.5 Ma, and 263.5 ± 2.8 Ma, respectively, indicating that the youngest sandstones were tectonic emplaced in the Houhongquan ophiolitic mélange after ca. 222 Ma. The sandstone matrices display two types of age spectra. Early Permian sandstones have a single Devonian to Early Permian peak age patterns, indicating the existence of an independent Permian intraoceanic arc. In contrast, Late Triassic sandstones have multiple peaks with some Precambrian zircons, suggesting that they were sourced from a continental arc. Accordingly, we consider that the Houhongquan ophiolitic mélange tectonic was emplaced in the intraoceanic island arc during the Middle Permian and docked to a continental margin arc during the Late Triassic. Thus, we argue that the terminal amalgamation timing of the southern Altaids was probably during ca. 222–217 Ma.

1. Introduction

The Altaids (or Central Asian Orogenic Belt) is the largest accretionary orogenic collage in the Phanerozoic [1–3] (Figure 1(a)). It is formed by numerous different tectonic terranes, including intra-oceanic/island arcs, microcontinents, oceanic plateaus, and accretionary prisms in the

Phanerozoic [3–6]. The Altaids was formed by consumption of the Paleo-Asian Ocean along the South Tianshan–Beishan–Solonker suture zone at the south Altaids [3, 6]. Nevertheless, the final accretionary and amalgamation processes are controversial, varying from the Devonian [7–11] to Triassic [6, 12–14] in different ophiolitic belts. Accordingly, the Beishan orogen, the middle segment of the Tianshan–

Beishan–Solonker suture zone, is critical for manifesting the accretionary tectonics and addressing the final time of amalgamation [11, 13, 15, 16].

The Beishan orogen comprises of several continental arcs, intraoceanic arcs, and accretionary prisms [16]. Although previous studies have established several evolution models for the multiblock accretion and their amalgamation processes, the tectonic and evolution in space during the Devonian to Triassic are still debatable. Both subduction settings [16–19] and postcollisional rifting [9, 10, 20, 21] have been proposed. In the southern Beishan orogen, voluminous Devonian to Triassic magmatism, sedimentary rocks developed in the Liuyuan accretionary complex belt, which is critical for constraining the tectonic of the Beishan orogen. In past decades, several studies have obtained the ages (~286 Ma to 270 Ma) of gabbros in this belt, but the closure of the Liuyuan–Houhongquan Ocean has not been constrained [9, 16, 22]. The age of the matrices of an accretionary complex is used for constraining the subduction processes, with the youngest matrices close to the final amalgamation time [23]. The spectra of the detrital zircon usefully constrain the sedimentary provenance [24, 25] and its maximum depositional age (MDA) [26–29]. Therefore, the MDA of matrices of the *mélange* is a valuable method to study the emplacement processes of accretionary complexes.

This study reports new field mapping of the Houhongquan ophiolitic *mélange* in the Beishan orogen. We also present new geochronological data of the sandstone matrices and geochemical data of mafic rocks from the ophiolitic *mélange*, aiming to reveal the accretion process of the Houhongquan ophiolitic *mélange* and put new constraints on the final amalgamation history of the south Altai.

2. Geological Backgrounds

The Beishan orogen consists of several WE-trending tectonic units, which are bounded by four ophiolitic *mélanges* (or accretionary complex) as illustrated in Figures 1(b) and 1(c) [11, 16]. The Houhongquan ophiolitic *mélange* is situated at the eastern segment of the Liuyuan accretionary complex situated between the Huaniushan and Shibanshan arcs (Figures 1(b) and 1(c)).

The Huaniushan arc comprises a set of Precambrian to Permian gneisses, migmatites, schists, sedimentary rocks, and carbonates [11, 16, 30, 31] and Ordovician–Permian arc-related basalt, andesite, rhyolite, and pyroclastic rocks [8, 13, 16, 32]. The sandstones, schists, and mylonites have the maximum depositional ages (MDA) of 293 to 457 Ma [9, 33, 34]. Extensive intrusions are ages from the Ordovician to Triassic, including I-, S-, and A-type granites, adakitic granites, and (ultra-)mafic intrusions (Figure 1(c) and Supplementary Table 2) [8, 9, 18, 22, 35–37].

The Shibanshan arc is the southernmost terrane of the Beishan orogen rooted in the Dunhuang block (Figures 2(b) and 2(c)). Two units constitute the Shibanshan arc: late Paleozoic volcanic-sedimentary unit and the metamorphic Beishan complex unit. The late Paleozoic volcanic-sedimentary unit, which is located at north Shibanshan arc, consists of Devonian–Permian arc-related volcanic

rocks, sedimentary rocks, and some carbonates [8, 11, 16]. The Beishan complex unit comprises migmatites, gneisses, (mylonitic) schists, and marbles, with MDAs of 1450–254 Ma and volumes of Precambrian zircons (Figure 1(c) and Supplementary Table 2) [19, 20, 38]. Some Precambrian schists have also been discovered in this unit [10, 20, 39]. The arc-related granites are extensive in the two units and dated from the Carboniferous to Triassic (Figure 1(c) and Supplementary Table 2) [8, 40, 41].

The Liuyuan accretionary complex comprises the Gubaoquan eclogites as well as the Huitongshan, Huaniushan, Liuyuan, Houhongquan, and Zhangfangshan ophiolitic *mélange* from west to east. The ophiolitic *mélanges* are composed of ultramafic rocks, gabbros, basalts, cherts, sedimentary rocks, and limestones [9, 13, 16, 42]. The age of the ophiolitic fragments and eclogites varies from 1071 Ma to 270 Ma (Supplementary Table 2). The Liuyuan–Houhongquan mafic-sedimentary rock belt is located along the Liuyuan accretionary complex from Liuyuan to Houhongquan area. The Houhongquan area is well exposed in the eastern segment of this belt (Figures 1(c) and 2). It consists of gabbro, pillow basalt, massive basalt, cleavage basalt, chert, sedimentary rock, and some andesite to dacite block [9, 13, 43]. The gabbros of the Liuyuan area and Yinaoxia area have ages ranging from 270 to 286 Ma [9, 13, 44]. The cherts are of biochemical origin (contain radiolarians and sponge spicules) and deposited in the pelagic environment near a continental margin [43]. The sedimentary rocks have the MDAs of 293 Ma to 234 Ma [9, 45]. To date, the genesis of these basalts and gabbros is strongly debated: one model suggests that they are the ophiolitic remnants [13, 16], whereas another model proposed that these magmatic and sedimentary rocks formed in the rift [8, 9, 46] and were thrust southward during 230–227 Ma [9] or in a back-arc setting [34] during 300–230 Ma and were thrust southward during 270–217 Ma [34].

3. Field Observations and Sampling

The Houhongquan ophiolitic *mélange* was exposed within the Mesozoic–Cenozoic sediments. The Houhongquan ophiolitic *mélanges* have the typical block-in-matrix structure (Figures 2 and 3). Altered gabbros, massive and pillow basalts, and chert fragments (Figure 4) and cleaved conglomerate, sandstone, and siltstone blocks (Figure 5) were thrust-imbricated into NEE-trending dismembered slices (Figures 2(c) and 2(d)). Volumes of basaltic and gabbroic fragments embraced in the cleaved sandstones (Figures 4(b) and 4(c)). The basaltic fragments that are close to the fault are strongly cleaved (Figure 4(c)). Usually, chert fragments are imbricated into basalts or occurred between basalts and sediments (Figures 2(c), 2(d), and 4(d)). The EW-trending granite fragments are located along faults (Figure 2). Sedimentary blocks are in fault contact with basalts (Figures 2(c) and 2(d)). The southwestern part sedimentary rocks are EW trending with S-dipping beddings and cleavages (Figures 2(b), 2(f), and 2(g)). However, the sedimentary blocks in the northern parts of the complex are EW-trending

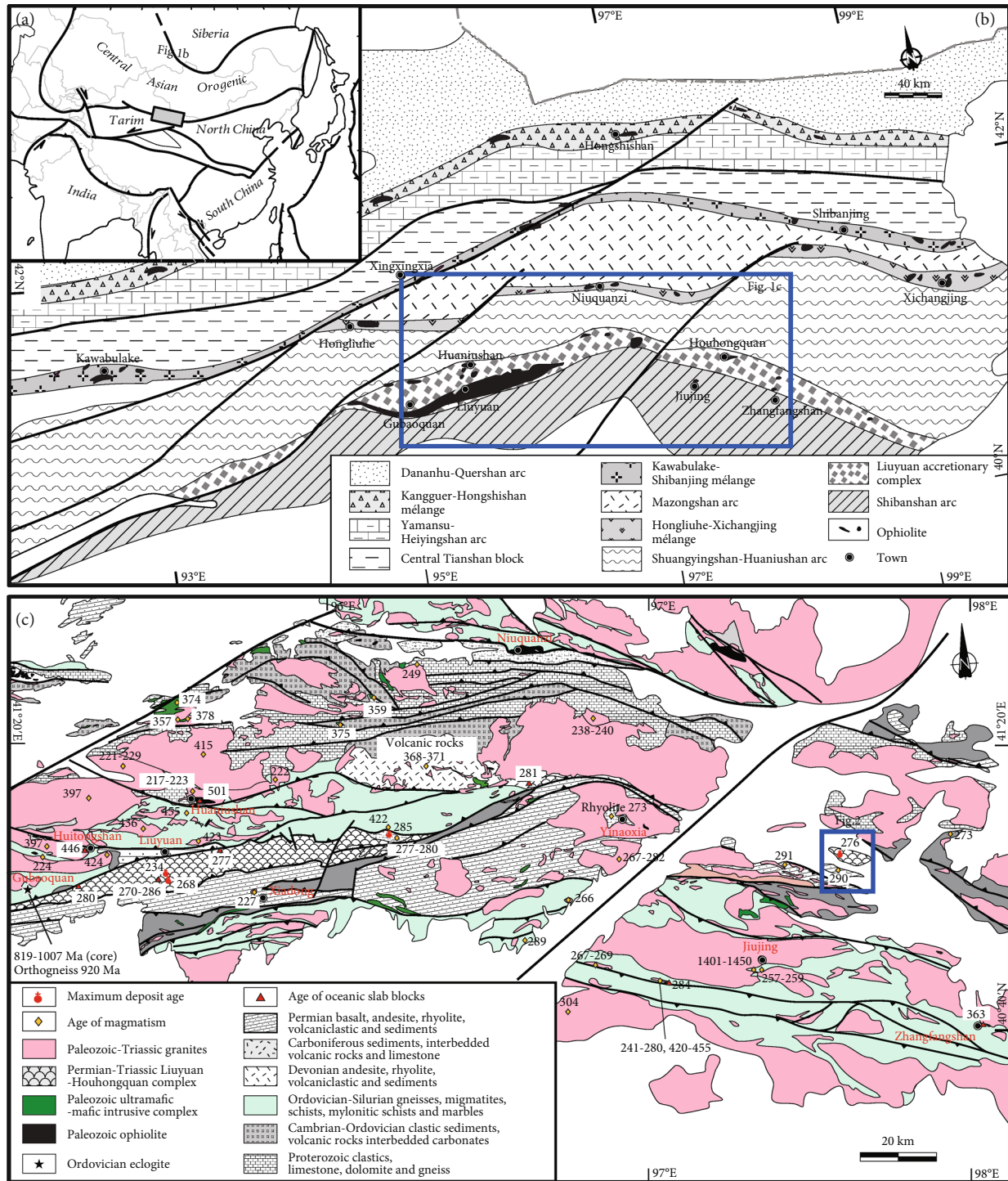


FIGURE 1: (a) Tectonic map of Altai and adjacent areas [2, 3] showing that the Beishan orogen is located at the southern Altai in (b). (b) Tectonic division map of Tianshan-Beishan orogenic belt [16]. (c) Geological map of south Beishan orogen. The Houhongquan ophiolitic mélangé is located at the eastern segment of the Liuyuan accretionary complex [13, 32]. The ages are cited in Supplementary Table 2.

with vertical N-dipping beddings and cleavages (Figures 2(b), 2(h), and 2(i)).

Some turbidites that consist of conglomerates, sandstones, siltstones, and mudstones can be well recognized in the outcrop (Figure 5). They are composed of conglomerate/gravel-bearing sandstones in the bottom (A layer, Figures 5(a) and 5(d)), followed by sandstones with a hori-

zontal bedding (B layer, Figures 5(a) and 5(b)), local cross-bedding (C layer, Figure 5(b)), and finally tuff siltstones, mudstones, and siliceous mudstones (D layer; Figures 5(b) and 5(c)). In general, siltstones and mudstones are highly cleaved (Figure 5(a)).

Thirteen basalts and six gabbros were picked (Figure 2) for geochemical studies. Two basalts and two gabbros were

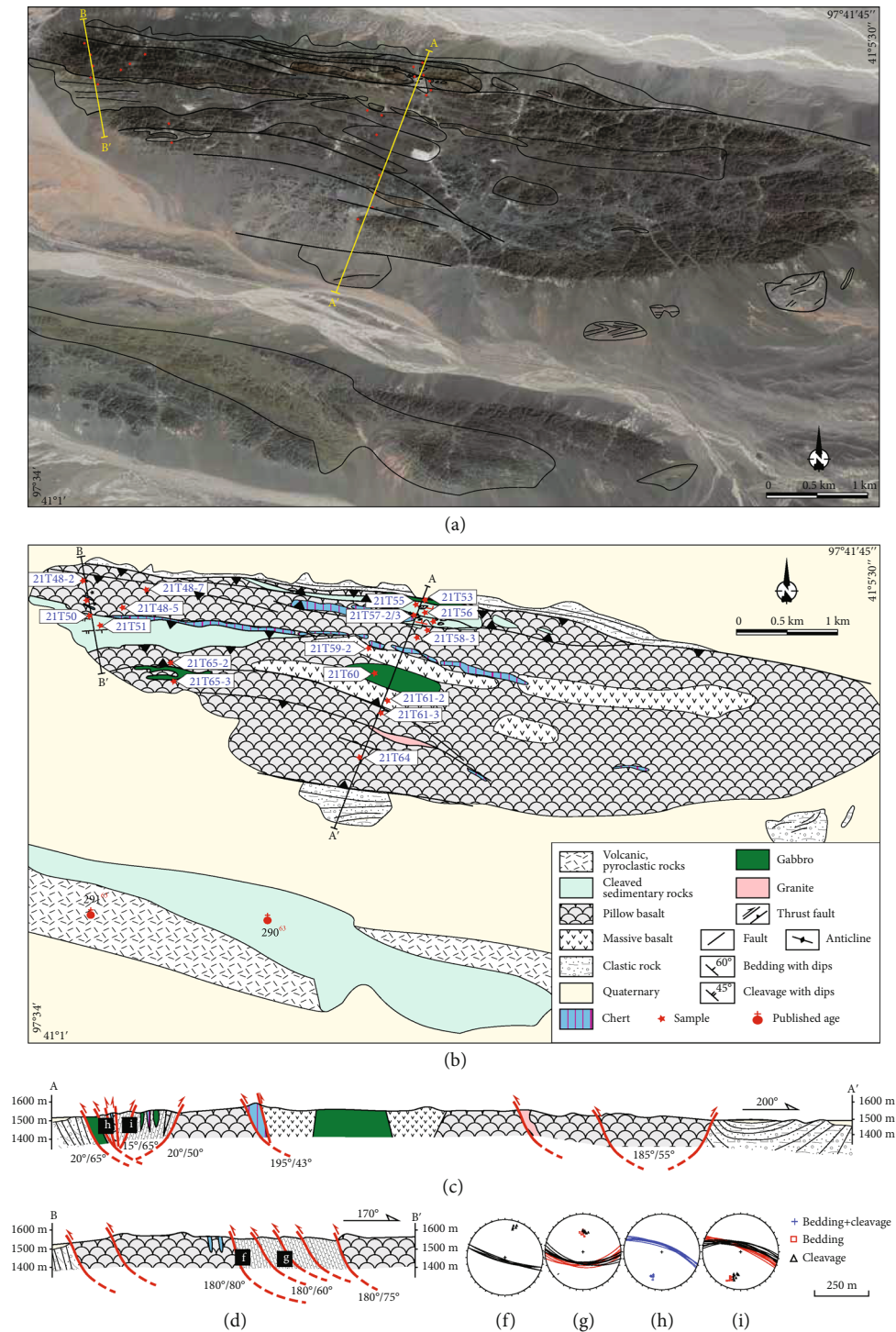


FIGURE 2: (a) Satellite image of the Houhongquan ophiolitic mélangé downloaded from Google Earth. (b) Geological map of the Houhongquan ophiolitic mélangé. (c, d) Geological cross-sections of the Houhongquan ophiolitic mélangé. (f–h) The pole plot diagrams for the bedding and cleavage of the sedimentary blocks. The pole plot of the foliations is on the lower hemisphere.

selected for Sr and Nd isotope analyses. Gabbro samples are grey and slightly altered (Figures 4(c) and 4(e)). They consist of medium-grained plagioclase (~50%) and pyroxene (~25%), as well as minor olivine and Fe–Ti oxides (Figure 4(e)). The basalts show variable degrees of chloritization, epidotization, and/or carbonation (Figures 4(a) and

4(b)). Locally, they have circular to elliptical amygdaloidal structures. The basalts consist of plagioclase, pyroxene, and minor olivine and a small amount of pyroxene phenocryst in some samples (Figure 4(f)).

As described above, the sedimentary blocks are composed of conglomerates, sandstones, siltstones, and

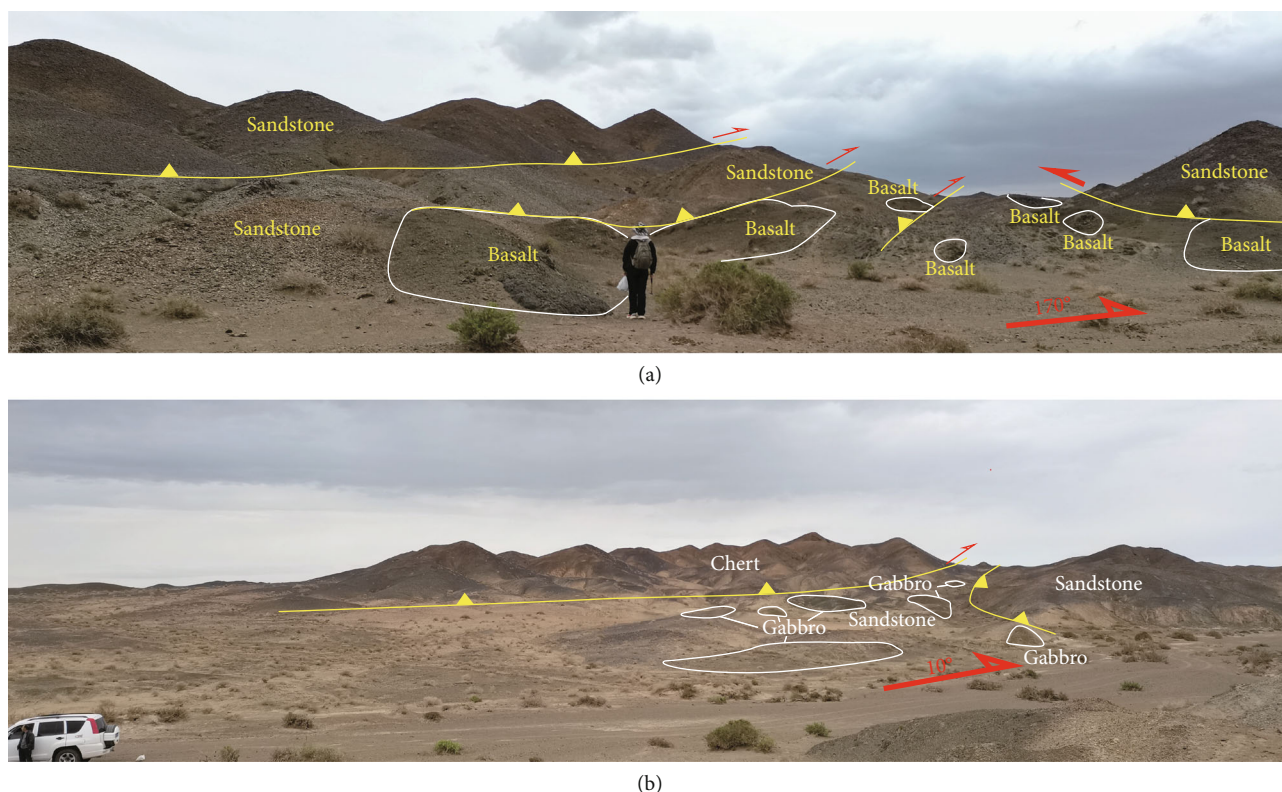


FIGURE 3: Photograph of the Houhongquan ophiolitic mélangé, showing the thrust-imbrication structures, and the basalt occurs as a tectonic block in the foliated matrix of sandstone.

mudstones. The conglomerates mainly consist of angular basalts, rhyolites, cherts, and minor quartz fragments (Figure 5(d)). The coarse-grained sandstones comprise angular plagioclase and basalt lithic fragments (e.g., sample 21T51, Figure 5(e)). The sandstones comprise of angular quartz, plagioclase, and minor lithic fragments (e.g., samples 21T50 and 21T55). The siltstones consist of quartz and tuff/clay (sample 21T56, Figure 5(f)).

4. Geochemical Results

4.1. Major and Trace Elements. The analysis results are presented in Table 1. The samples 21T48-7 and 21T57-5 are too altered ($LOI > 5\%$), and we have excluded them from the dataset. These rocks plot tholeiitic basalt as shown in Figure 6. The compositions of these mafic samples are slightly correlated (Supplementary figure 2).

Eleven basalt samples have a relatively wide content of SiO_2 (46.5–54.3 wt. %), Al_2O_3 (12.8–15.1 wt. %), CaO (8.2–15.9 wt. %), MgO (3.1–6.9 wt. %), and $Mg^\#$ values of 43–61. These basalts exhibit relatively moderate to high contents of TiO_2 (1.6–3.3 wt. %). They have a wide range of Cr (10–280 ppm) and Ni (6.6–62.3 ppm) contents. The basalts are slightly enriched in LREEs ($(La/Yb)_N = 1.2 - 2.2$) and have slightly negative Eu anomalies ($Eu^* = 0.8 - 1.0$) ([47], Figure 7(a)). The basalts can be divided into two distinct groups: one group has slight depletions of Nb and Ta ($Th/Nb_{PM} = 1.08 - 2.38$) (black lines in Figure 7(b)) whereas another group shows depletions of Th relative to Nb and Ta ($Th/Nb_{PM} = 0.86 - 0.96$) (red lines in Figure 7(b)).

Six gabbro samples have SiO_2 contents of 46.9 to 52.4 wt. %, and TiO_2 contents of 2.0 to 2.6 wt. %. They are characterized by Al_2O_3 ranging from 14.2 to 16.4 wt. %, CaO ranging from 7.3 to 9.3 wt. %, and MgO ranging from 4.3 to 4.5 wt. % ($Mg^\# = 46 - 63$), and $K_2O + Na_2O$ ranging from 3.4 to 5.3 wt. %. The gabbro samples have Cr and Ni contents of 70–210 ppm and 32–64 ppm. They show slight enrichment in LREEs ($(La/Yb)_N = 1.7 - 2.7$) and weak Eu anomalies ($Eu^* = 0.9 - 1.0$) in the chondrite-normalized REE diagram ([48]; Figure 7(c)). The gabbro samples also exhibit two distinct groups [46]: one group shows slight depletions of Nb and Ta ($Th/Nb_{PM} = 1.45 - 1.61$) (black lines in Figure 7(d)), whereas another group shows depletion patterns ($Th/Nb_{PM} = 0.85 - 0.96$) (red lines in Figure 7(d)).

4.2. Sr–Nd Isotopes. The results of Sr and Nd isotopic analyses are summarized in Table 2 and shown in Figure 8. Two basalt samples have $(^{87}Sr/^{86}Sr)_i$ values of 0.704748 and 0.704859 and $\epsilon_{Nd}(t)$ values of +6.2 and +6.3, respectively. The two gabbro samples have $(^{87}Sr/^{86}Sr)_i$ values of 0.705602 and 0.705863 and $\epsilon_{Nd}(t)$ values of +5.8 and +6.0. Because the samples are slightly altered by the seawater (e.g., chloritization, epidotization), the Sr isotopes moved along the trend of the seawater alteration (Figure 8) [49].

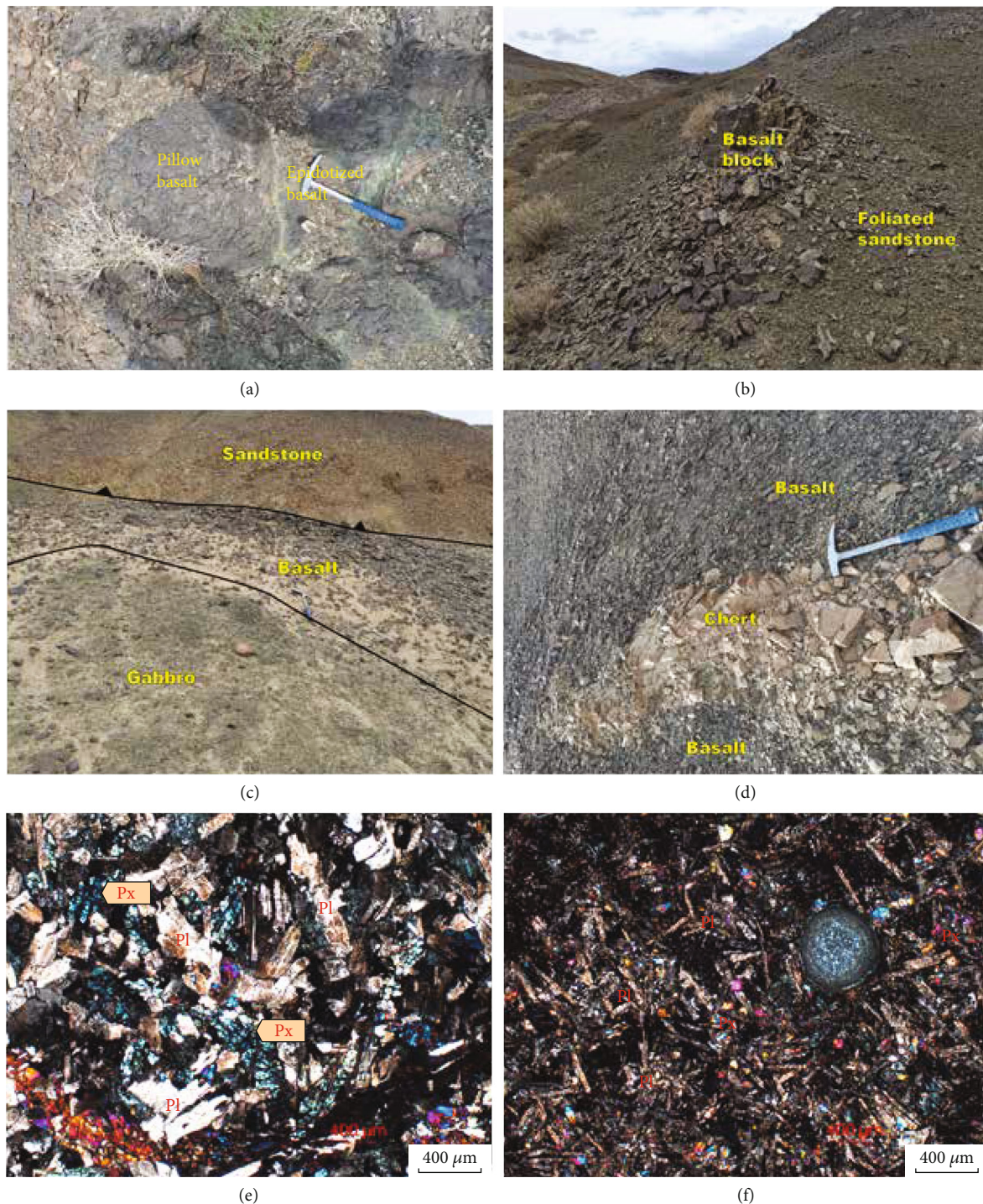


FIGURE 4: Photograph and photomicrographs of the oceanic and granite blocks: (a) pillow basalt; (b) basalt fragment in foliated sandstone matrix; (c) basalt block in sandstone; (d) chert block in basalt; (e) photomicrograph of gabbro which mainly consists of pyroxene and plagioclase; (f) photomicrograph of basalts; the circular structure is amygdaloidal. Pl: plagioclase; Px: pyroxene.

5. Zircon U–Pb Ages

Overall, 393 analyses of zircons from four sedimentary samples yielded 374 concordant ages (concordance% > 90% or < 110%). Different methods are suggested to constrain the MDA of sedimentary rocks in international community

[26, 27], including the youngest one, the three youngest grains, and the youngest peak. Here, we adopt the weight mean age of the three youngest grains if they overlap at a 2σ uncertainty or the youngest one if the weight mean age of the three youngest zircons far exceed the 2σ uncertainty (MWSD is poor).



FIGURE 5: Photograph and photomicrographs of the sedimentary matrix: (a–c) photographs of turbidite; the siltstone and mudstone are cleaved; (d) conglomerate; (e, f) photomicrographs of lithic sandstone, siltstone, and mudstone. Q: quartz; Pl: plagioclase; L: lithic fragment.

5.1. Sample 21T50. The zircons of the sample 21T50 are euhedral, and some are slightly rounded. They range in length of 50–120 μm with length/width ratios of 1.2–2.0, with oscillatory zones (Figure 9(a)). They have Th/U values of 0.18–2.49. One hundred grains were analysed, and ninety grains yield concordant ages with a multi-peak spectrum and peaks ca. 268 Ma (~43.3%) and ca. 390 Ma (~40.1%) and some Precambrian ages scattered at 615 Ma, 878 Ma, 1246 Ma, and 2144 Ma (Figure 9(b)). The youngest three zircons (222 \pm 5 Ma, 235 \pm 3 Ma, and 235 \pm 5 Ma) yield a weight mean age of 232 \pm 16 Ma (Figure 9(a)); however, the MWS is poor (MWS = 10), so we suggest that the MDA of the sandstone is the youngest zircon grain (222 Ma).

5.2. Sample 21T55. Zircons from sample 21T55 in the eastern part of the Houhongquan ophiolitic mélangé are euhedral and are 50–150 μm long. They display oscillatory zonation (Figure 9(c)) and Th/U ratios of 0.09–2.61. Ninety-nine grains of 100 analysed grains yielded concordant ages with a multi-peak spectrum. The two major peaks are at ca. 262 Ma (~63.3% of the total) and ca. 398 Ma (~29.3%) (Figures 9(c) and 9(d)). There are eight Precambrian zircon ages ranging from 902 Ma to 2484 Ma (~7.4%). The three youngest zircons yield 233.8 \pm 2.3 Ma (MSWD = 0.39) (Figure 9(c)), indicating the MDA of the sandstone.

5.3. Sample 21T51. Zircons from sample 21T51 have irregular lengths of 50–120 μm and clear oscillatory zoning

TABLE 1: Geochemical results of basalts and gabbro from the Houhongquan ophiolitic mélange.

Sample No.	21T48-2	21T48-3	21T48-7	21T58-2	21T58-3	21T59-2	21T61-3	21T64-2	21T65-2	21T65-3	21T65-5	21T61-2	21T53-2	21T57-2	21T57-3	21T60-2	21T60-3	
Rock type	Basalt	Basalt	Basalt	Basalt	Basalt	Basalt	Basalt	Basalt	Basalt	Basalt	Basalt	Basalt	Gabbro	Gabbro	Gabbro	Gabbro	Gabbro	
SiO ₂	50.39	48.42	50.61	50.94	47.85	47.90	54.25	50.56	46.51	49.14	48.28	47.17	50.92	46.91	47.24	50.61	49.84	50.58
TiO ₂	1.88	1.97	1.62	2.19	2.20	1.59	2.39	3.28	1.55	1.62	2.30	1.87	2.50	2.05	2.34	2.03	2.57	2.43
Al ₂ O ₃	14.22	14.90	12.58	14.42	13.76	15.12	13.36	12.84	14.36	14.42	14.40	15.70	13.93	16.28	15.82	16.44	14.24	14.42
CaO	9.09	10.30	11.35	8.78	8.36	11.40	9.47	8.21	15.90	11.05	10.10	9.25	10.45	9.25	9.29	8.54	7.88	7.34
Fe ₂ O _{3T}	10.70	9.95	9.91	10.96	14.27	10.08	9.51	12.31	9.59	10.35	12.11	8.45	11.99	10.43	10.67	8.93	8.28	12.44
MnO	0.17	0.19	0.14	0.18	0.18	0.19	0.26	0.14	0.16	0.18	0.22	0.45	0.23	0.18	0.18	0.21	0.23	0.37
MgO	6.92	6.31	4.13	6.30	6.42	6.84	3.09	4.65	3.69	4.25	6.14	4.86	4.07	6.48	6.30	6.28	6.04	5.31
K ₂ O	0.43	0.50	0.15	0.63	0.72	0.49	0.19	0.07	0.06	0.14	0.94	0.39	0.14	0.36	0.65	0.55	0.66	0.10
Na ₂ O	2.44	3.54	4.16	3.61	3.98	2.81	3.81	4.96	3.28	4.83	2.81	5.19	3.74	3.89	3.72	2.87	2.91	5.23
P ₂ O ₅	0.25	0.24	0.24	0.25	0.23	0.19	0.29	0.53	0.22	0.24	0.28	0.32	0.30	0.29	0.30	0.33	0.34	0.39
LOI	3.62	4.09	5.31	2.15	2.55	3.14	3.08	2.49	4.73	3.81	2.75	6.42	2.05	4.54	3.38	3.75	3.05	2.40
Total	100.11	100.41	100.20	100.41	100.52	99.75	99.70	100.04	100.05	100.03	100.33	100.07	100.32	100.66	99.89	100.54	99.79	100.23
Mg [#]	60.11	59.64	49.27	57.26	51.18	61.26	43.09	46.82	47.28	48.90	54.16	57.27	44.17	59.15	57.91	62.11	62.96	49.87
Sc	41.9	42.8	34.8	42.8	42.5	39.6	42.0	33.4	30.5	31.7	45.7	29.8	43.7	36.7	36.1	32.4	30.2	38.6
V	330	361	299	355	377	285	372	362	318	303	364	251	397	292	334	270	266	333
Cr	170	190	190	120	120	280	40	10	180	180	100	170	40	210	190	180	170	110
Co	37.5	38.8	27.9	34.6	39.4	42.6	39.5	19.0	31.5	29.6	41.6	35.0	39.1	35.2	32.3	31.1	30.4	35.4
Ni	57.1	58.8	45.6	45.4	38.2	56.7	23.3	6.6	62.3	55.2	33.6	62.4	23.8	63.6	55.1	58.3	59.0	31.9
Cu	33.5	37.2	27.7	24.8	27.3	10.2	59.5	15.0	33.8	35.7	38.4	39.5	63.1	44.4	50.4	97.0	60.9	25.3
Zn	86	93	52	98	102	85	98	57	62	71	97	70	120	80	78	73	70	87
Ga	20.3	21.5	13.10	20.1	19.20	18.40	20.2	26.8	22.6	17.15	20.3	18.40	21.5	20.8	20.5	21.1	20.3	21.4
Rb	4.9	6.2	1.5	16.6	18.7	11.1	1.0	0.6	0.7	1.6	17.1	9.1	0.6	4.2	6.9	5.2	6.7	0.9
Sr	295	208	138.0	231	215	181.0	285	171.0	120.5	189.5	336	276	268	195.0	154.5	288	297	178.0
Y	37.4	36.7	31.6	43.2	42.6	31.5	41.4	95.8	30.0	32.4	40.3	31.2	43.3	33.3	34.3	34.3	35.1	49.5
Nb	5.3	5.3	4.5	3.8	3.7	3.3	4.6	7.8	5.1	5.3	4.6	7.2	4.8	7.0	7.4	7.8	8.0	5.8
Cs	0.26	0.26	0.28	0.57	0.68	0.47	0.08	0.05	0.14	0.13	0.54	0.43	0.04	0.21	0.22	0.38	0.38	0.04
Ba	85.4	71.0	33.3	37.2	44.2	69.4	67.7	17.6	40.6	27.3	130.0	291	33.3	43.8	56.9	75.8	81.2	21.8
La	8.4	8.3	7.2	6.6	6.7	5.2	8.0	19.2	8.8	9.3	7.5	8.9	8.0	10.3	10.3	11.8	11.8	10.5
Ce	23.3	23.5	20.4	20.2	20.4	15.4	23.4	50.5	22.6	23.4	24.4	26.0	24.3	27.4	27.9	30.3	30.9	30.2
Pr	3.57	3.58	2.99	3.37	3.27	2.51	3.75	7.64	3.28	3.44	3.63	3.87	3.94	4.00	4.10	4.37	4.48	4.68
Nd	17.5	17.2	14.7	17.7	17.2	12.9	19.2	39.1	15.4	16.3	18.3	18.4	20.0	18.5	19.2	20.4	20.8	23.4
Sm	5.01	4.99	4.17	5.47	5.31	3.97	5.55	11.70	4.24	4.52	5.28	4.75	5.98	4.94	5.13	5.27	5.36	6.82
Eu	1.85	1.82	1.50	2.05	2.01	1.48	2.08	3.56	1.50	1.53	1.99	1.56	2.16	1.79	1.83	1.90	1.87	2.38
Gd	6.67	6.65	5.51	7.42	7.35	5.42	7.28	15.60	5.47	5.62	7.12	5.82	7.82	6.19	6.36	6.28	6.44	8.55
Tb	1.08	1.07	0.91	1.24	1.21	0.87	1.16	2.56	0.87	0.91	1.15	0.94	1.24	0.99	1.00	1.00	1.00	1.38
Dy	6.93	6.83	5.71	7.78	7.92	5.78	7.74	16.70	5.55	5.87	7.53	5.75	8.06	6.24	6.38	6.25	6.38	8.86
Ho	1.39	1.39	1.16	1.58	1.61	1.17	1.55	3.45	1.13	1.18	1.51	1.17	1.63	1.24	1.29	1.27	1.28	1.81
Er	3.93	3.96	3.33	4.43	4.55	3.27	4.39	9.91	3.23	3.31	4.13	3.26	4.54	3.48	3.55	3.61	3.53	5.12

TABLE 1: Continued.

Sample No.	21T48-2	21T48-3	21T48-7	21T58-2	21T58-3	21T59-2	21T61-3	21T64-2	21T65-2	21T65-3	21T48-5	21T57-5	21T61-2	21T53-2	21T53-3	21T57-2	21T57-3	21T60-2	21T60-3
Rock type	Basalt	Basalt	Basalt	Basalt	Basalt	Basalt	Basalt	Basalt	Basalt	Basalt	Basalt	Basalt	Basalt	Basalt	Basalt	Basalt	Basalt	Basalt	Basalt
Tm	0.59	0.58	0.49	0.66	0.68	0.49	0.65	1.49	0.47	0.50	0.63	0.48	0.68	0.52	0.53	0.53	0.53	0.75	0.90
Yb	3.54	3.49	3.02	3.89	4.09	2.95	3.90	9.10	2.89	3.01	3.74	2.90	4.05	3.17	3.19	3.26	3.20	4.56	5.33
Lu	0.56	0.55	0.47	0.62	0.66	0.48	0.64	1.46	0.46	0.48	0.61	0.45	0.65	0.50	0.52	0.51	0.50	0.72	0.86
Zr	1.78	1.79	1.45	1.64	1.66	1.25	1.91	3.91	1.48	1.53	1.94	1.94	1.98	1.93	2.00	2.16	2.23	2.29	2.72
Hf	4.2	4.2	3.4	4.2	4.1	3.2	4.6	9.4	3.6	3.7	4.6	4.4	4.8	4.2	4.5	4.8	4.8	5.3	6.4
Ta	0.39	0.39	0.32	0.26	0.26	0.23	0.31	0.56	0.32	0.35	0.37	0.48	0.32	0.49	0.48	0.57	0.54	0.41	0.46
Pb	1.9	2.0	1.8	1.6	2.0	1.6	2.2	3.4	3.4	2.4	1.9	2.0	1.0	1.7	1.8	1.8	2.1	1.4	1.1
Th	0.93	0.90	0.80	0.76	0.77	0.56	0.59	2.21	1.00	1.00	0.48	0.77	0.55	0.74	0.76	0.88	0.91	1.00	1.36
U	0.27	0.27	0.20	0.75	0.31	0.22	0.51	0.94	0.22	0.18	0.24	0.50	0.22	0.34	0.30	0.33	0.55	0.54	0.69
Mg [#]	60.1	59.6	49.3	57.3	51.2	61.3	43.1	46.8	47.3	48.9	54.2	57.3	44.2	59.1	57.9	62.1	63.0	49.9	46.3

Mg[#] = (Fe₂O₃ / T * 0.8998 / 71.85 * (1 - 0.15)) * 100; Eu * = EuN/SQRT(SmN * GdN).

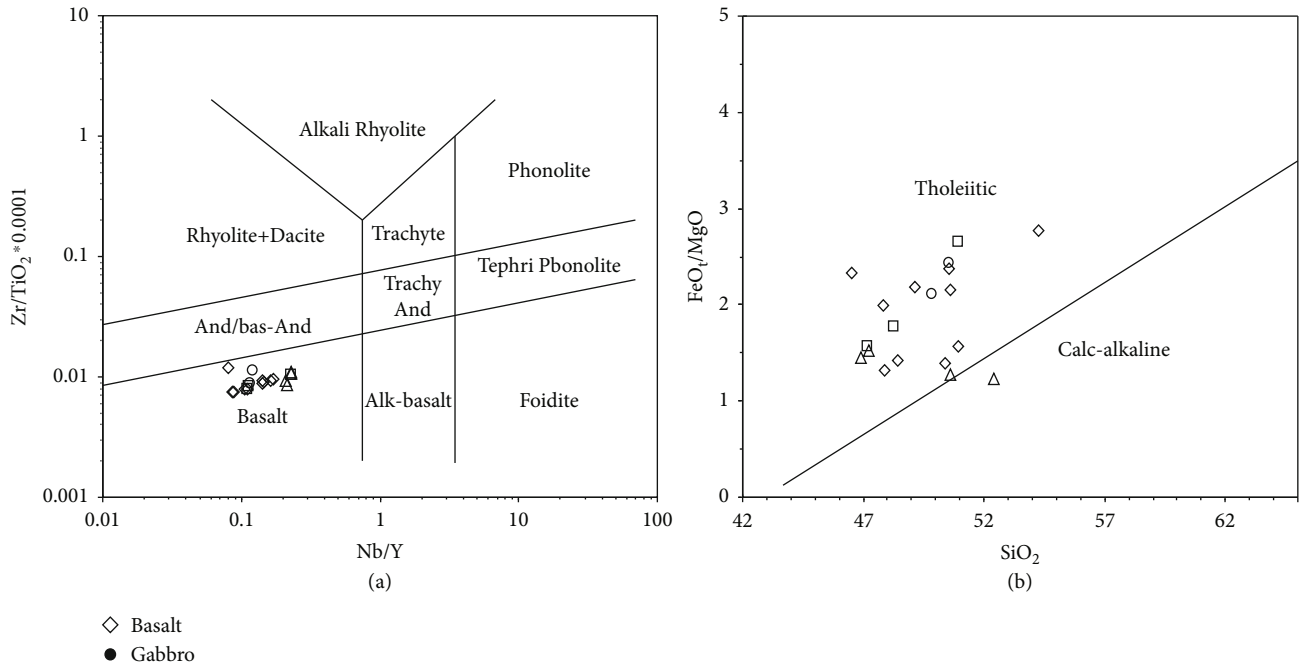


FIGURE 6: (a) Zr/Ti vs. Nb/Y [80] and (b) FeO/MgO vs. SiO_2 [81] geochemical classification diagrams for the Houhongquan ophiolitic mélangé.

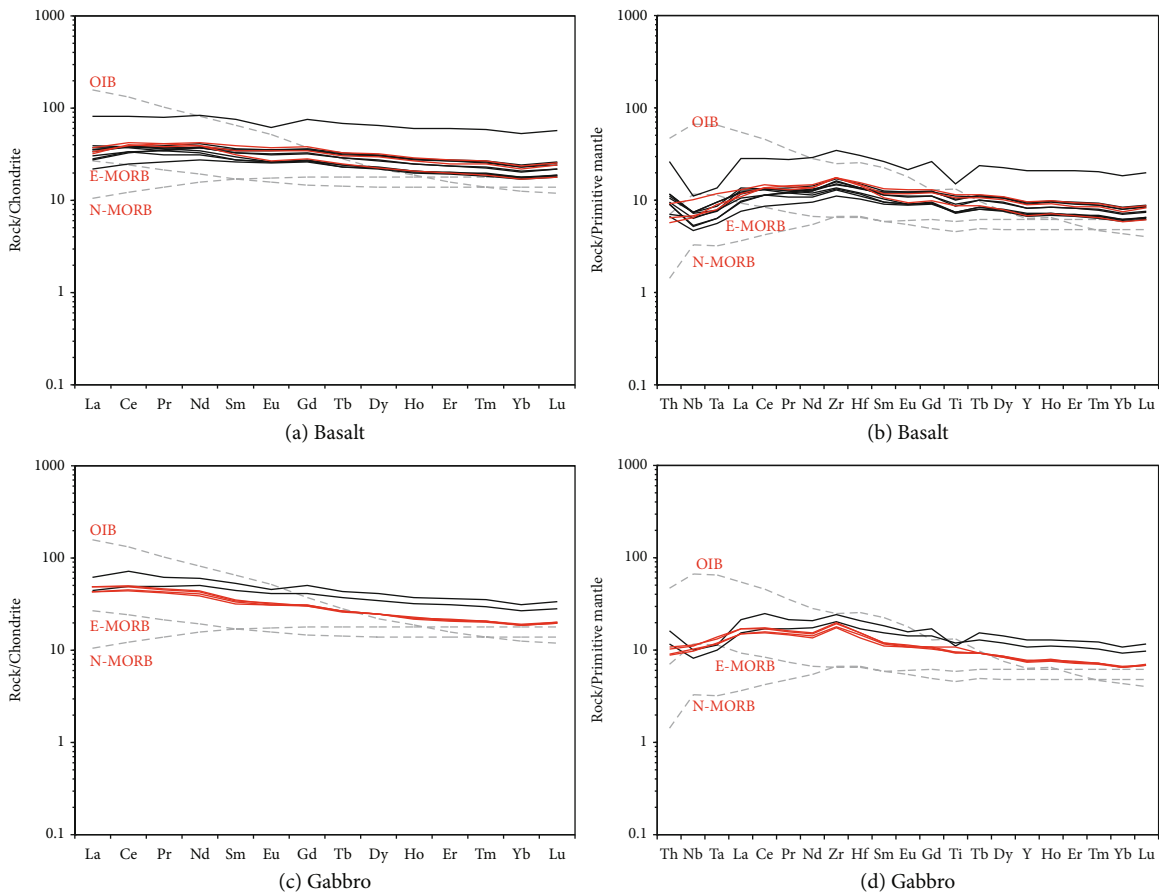


FIGURE 7: Chondrite-normalized REE and primitive mantle-normalized multielement diagrams of mafic rocks from the Houhongquan ophiolitic mélangé. The chondrite data are from Boynton [47]. The primitive mantle, N-MORB, E-MORB, and OIB values are from Sun & McDonough [48].

TABLE 2: Sr-Nd isotope results of basalts and gabbro from the Houhongquan ophiolitic mélange.

Sample	Rock type	Age (Ga)	Rb	Sr	$^{87}\text{Rb}/^{86}\text{Sr}$	$^{87}\text{Sr}/^{86}\text{Sr}$	2s	$(^{87}\text{Sr}/^{86}\text{Sr})_i$	Sm	Nd	$^{147}\text{Sm}/^{144}\text{Nd}$	$^{143}\text{Nd}/^{144}\text{Nd}$	2s	$(^{143}\text{Nd}/^{144}\text{Nd})_i$	ϵ_{Nd}
21T48-3	Basalt	285	4.5	193.5	0.0668	0.70502	0.000006	0.704748	4.3	15.3	0.1702	0.51291	0.00001	0.51259048	6.2
21T61-2	Basalt	285	1.0	300.9	0.0093	0.70490	0.000005	0.704859	5.9	19.6	0.1813	0.51293	0.000007	0.512592774	6.3
21T53-2	Gabbro	285	3.8	206.5	0.0533	0.70608	0.000005	0.705863	4.8	18.2	0.1599	0.51288	0.000009	0.512576613	6.0
21T57-5	Gabbro	285	7.7	298.4	0.0750	0.70591	0.000005	0.705602	4.6	17.2	0.1613	0.51287	0.000008	0.512566057	5.8

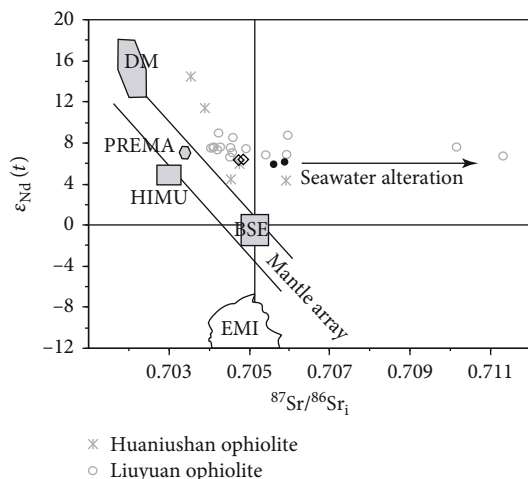


FIGURE 8: $\epsilon_{\text{Nd}}(t)$ vs. initial $(^{87}\text{Sr}/^{86}\text{Sr})_i$ for the basalt and gabbro of the Houhongquan ophiolitic mélangé. DM is depleted mantle; BSE is bulk silicate earth; EMI and EMI are enriched mantle; HIMU is mantle with high U/Pb ratio; PREMA is frequently observed prevalent mantle composition [82]. The Sr–Nd isotope data of the Liuyuan ophiolite are after Mao *et al.* [13], and those of Huaniushan ophiolite are after Mao *et al.* [64].

(Figure 9(e)). The analysed zircons show Th/U ratios of 0.36–1.49.87 concordant grains (~96%) displaying two major peaks at ca. 270 Ma (~86.7%) and ca. 402 Ma (~11.1%). Only two Precambrian zircons have 740 Ma and 1040 Ma, respectively (Figures 9(e) and 9(f)). The youngest three zircon ages yield 263.5 ± 2.8 Ma (MSWD = 0.001) (Figure 9(e)), which represent the MDA for the sandstone.

5.4. Sample 21T56. Zircons from sample 21T56 are euhedral which are 80–120 μm long (length/width = 1–1.5), with sharp oscillatory zones (Figure 9(g)). Their Th/U values vary from 0.60 to 1.70. Ninety-eight concordant analysed grains (98%) have a single peak at ca. 270 Ma (~99% of the total) (Figure 9(h)). The three youngest zircons yield 263.4 ± 2.5 Ma (MSWD = 0.06) (Figure 9(g)), which is the MDA of the sandstone matrix.

6. Discussion

6.1. Tectonic Setting of the Oceanic Components. The basalt and gabbro are tholeiitic magma with relatively high $\epsilon_{\text{Nd}}(t)$ (+5.8–+6.3 and low $(^{87}\text{Sr}/^{86}\text{Sr})_i$ (0.704748–0.70563) (Figure 8) ([45, 50], this study), suggesting that they were sourced from the depleted mantle. However, their geochemical data also indicate that these mafic blocks are derived from the different types or ages of oceanic crust. The compositions of the samples are uncorrelated, suggesting they have different sources (supplementary figure 2). Their slight enrichment of LREE (Figures 7(a) and 7(c)) is like that of E-MOR- and SSZ-type ophiolites. They also display back-arc basin basalts (BABB) and N-MORB geochemical signatures with slight depletions of Nb-Ta compared to the Th and La ($\text{Th}/\text{Nb}_{\text{PM}} = 1.08 - 2.38$) and depletions of Th relative to Nb and Ta ($\text{Th}/\text{Nb}_{\text{PM}} = 0.86 - 0.96$) (Figures 7(b) and 7(d)) [51, 52]. They are also plotted in

the N-MORB/BAB MORB realm on the V–Ti/1000 diagram ([53], Figure 10(a)). On the Hf–Th–Ta diagram ([54], Figure 10(b)), they are plotted in the N-MORB field and the arc-related basalt field, which coincide with the Lau Basin and Mariana Trough. All of these suggest that mafic fragments are composed of N-MOR- and SSZ-type ophiolites.

6.2. Age of the Houhongquan Ophiolitic Mélangé. Previous works have tried to place a constraint on the age of the Houhongquan ophiolitic mélangé, but none of them have been successful. Moreover, these rocks were considered coherent strata instead of being part of the tectonic mélangé, and their ages were constrained by the felsic rocks around the Houhongquan ophiolitic mélangé according to stratigraphic correlations of the regional sedimentary rocks [45, 50, 55]. For example, the rhyolite and the dacite south to the mélangé have zircon ages of 291.1 ± 2.6 Ma and 289.5 ± 2.3 Ma [50], and the calcareous sandstone has an age of 275.8 ± 1.4 Ma in the Houhongquan ophiolitic mélangé [45].

The detrital zircon age of the sedimentary rocks can provide a vital constraint on the MDA [27, 28]. The interval time between MDA and the true depositional age can be very short in the arc-related basins and accretionary prisms [26]. The clasts of conglomerates are mainly the angular chert, rhyolite, and basalt (Figure 5(d)), the coarse-grained sandstone contains the angular/broken basalt and rhyolite fragments (Figure 5(e)), and most of the zircons are euhedral and weak/not rounded (Figure 9), indicating they have proximal sources and deposited in the subduction zone [26, 56]. Therefore, the MDA of detrital zircons can represent the deposition time of these rocks [26]. The sandstone samples (21T50 and 21T55) yielded Late Triassic MDAs of 222 ± 5 Ma and 233.8 ± 2.3 Ma, respectively (Figures 9(a) and 9(b)). The sandstone samples (21T51 and 21T56) yielded Middle Permian MDAs of 263.5 ± 2.8 Ma and 263.4 ± 2.5 Ma, respectively (Figures 8(c) and 8(d)). In addition, Guo *et al.* [45] reported a calcareous sandstone in the Houhongquan ophiolitic mélangé, which has a MDA of 275.8 ± 1.4 Ma. All the results for each sample indicate that the ages of sedimentary blocks range from Middle Permian to Late Triassic. Previous geochronological studies for the gabbro of the Liuyuan–Houhongquan mafic-sedimentary rock belt revealed that they have ages of 270 Ma to 286 Ma [9, 13, 44] (Supplementary Table 2, Figure 11(a)). Some sedimentary blocks with MDAs of 234 Ma, 268 Ma, and 285 Ma (Figure 11(a)) were also reported in the Liuyuan–Houhongquan mafic-sedimentary rock belt [9]. Thus, the Liuyuan–Houhongquan Ocean still existed at 222 Ma. This conclusion is consistent with the rift model in which the Liuyuan basin closed during 230–227 Ma [9] and the back-arc basin model in which the Liuyuan back-arc basin closed until 217 Ma [34]. Therefore, no matter the Liuyuan–Houhongquan oceanic basin is a rift basin, a back-arc basin, or the Paleo-Asian Ocean, it did not closed until ca. 222 Ma.

6.3. Provenance of the Matrix. As discussed above, the components and petrology of the sandstones suggest they were

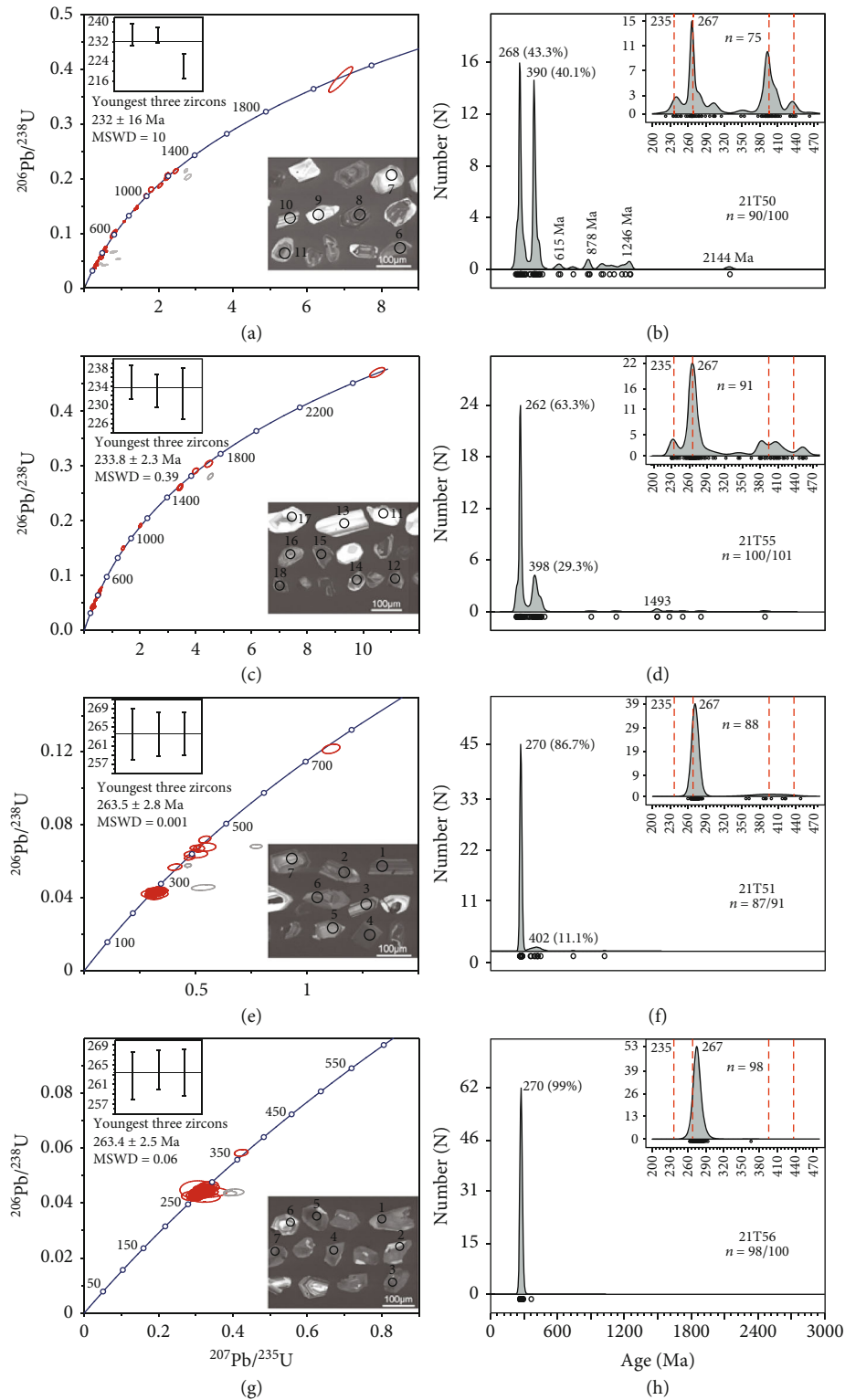


FIGURE 9: The concordia diagram contains the CL image (a, c, e, and g) and histograms (b, d, f, and h) for the sandstone matrix of the Huhongquan ophiolitic mélangé. Data are after Table 1.

sourced from the nearby arc [26, 56]. The Huhongquan ophiolitic mélangé is just positioned between the Huaniushan arc in the north and the Shibanshan arc in the south (Figure 1(b)). Previous studies revealed that the Hua-

niushan arc is a Japan-type arc during Early Ordovician-Permian, and the Shibanshan arc is an Early Devonian-Permian continental margin arc on the Dunhuang block [16, 35, 41]. They mainly comprise Triassic-Ordovician

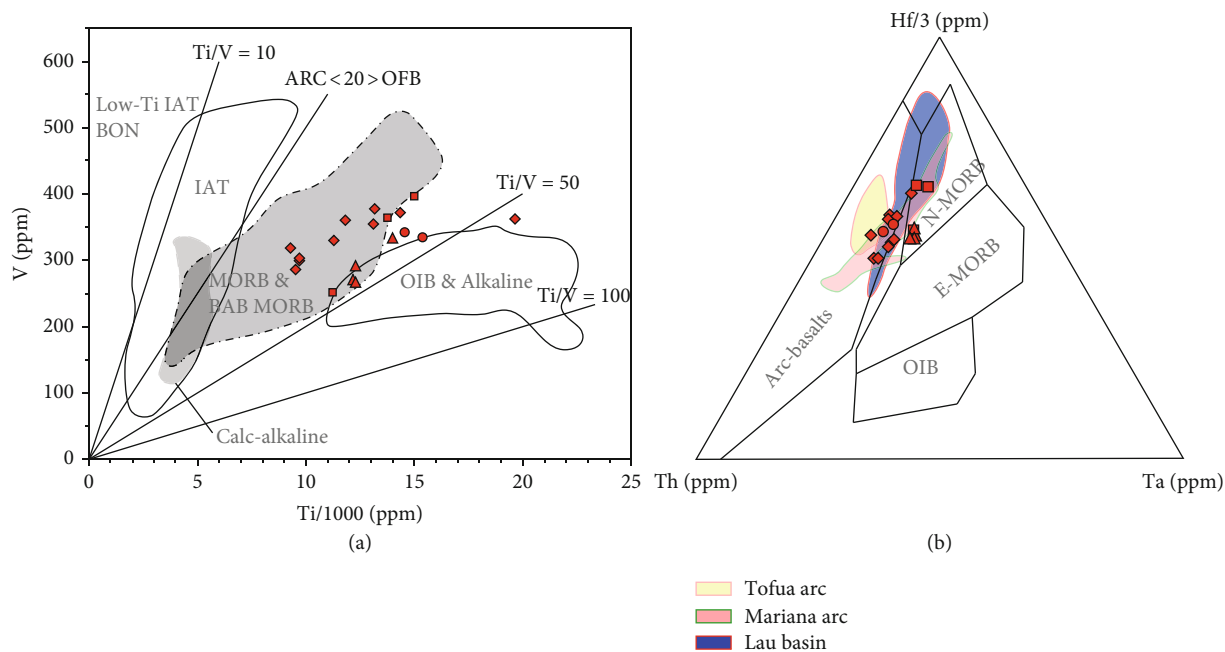


FIGURE 10: (a) V vs. Ti/1000 [53] and (b) Hf-Th-Ta [54] diagrams for the mafic rocks of the Houhongquan ophiolitic mélange. The Tofua Arc, Lau Basin, and Mariana Trough data are after Hawkins [83]. Symbols employed are the same as those in Figure 6.

arc-related basalts, andesites, rhyolites, and granitoids (Figures 2, 11(b) and 11(c); Supplementary Table 2) [18, 19, 22, 30, 41] and some Precambrian gneisses and schists [10, 20, 39]. Usually, the sedimentary rocks of the two arcs contain voluminous Precambrian zircon grains [19, 20, 31, 38, 57] (Figures 12(d), 12(f)–12(h)).

Our studies reveal that the sandstones (21T50, 21T51, 21T55, and 21T56) define two groups of age patterns. (1) The sedimentary samples (21T51 and 21T56) show Middle Permian MDAs with a single peak of ca. 274 Ma and a small amount of ages ranging from 362 Ma to 447 Ma (9 grains, ~5%) and minor Precambrian ages (2 grains, ~1%). These characteristics are like the detrital zircon age patterns of the sedimentary rock in intraoceanic arc setting, e.g., the Char and Zharma zones of eastern Kazakhstan [58], as well as the sediments of the Talkeetna arc in Alaska [59], of the Outer Melanesian Arc in the Fiji Islands behind the Tonga arc [60] and of the Izu-Bonin-Marianas arc [61]. These age compositions are different to the Permian sandstones in the Huaniushan arc and the Shibanshan arc (Figures 12(c), 12(e)–12(g)) but are consistent with two samples in the northern Shibanshan arc (Figure 12(d)). The detrital zircon age patterns of these sedimentary rocks suggest an intraoceanic arc in the Liuyuan–Houhongquan Ocean, which do not contain Precambrian zircon grains. Furthermore, the mafic rocks of the Houhongquan ophiolitic mélange plot in the same fields of Mariana arc and Lau Basin as shown in Figure 10(b), also suggesting that they deposited in the intraoceanic subduction zone. (2) Samples 21T50 and 21T55 have Triassic MDAs. Their detrital zircon age spectra are similar to the magmatic and sedimentary records from the Huaniushan arc and the Shibanshan arc with dominant age peaks from Triassic to Devonian and some scattered

Precambrian ages (Figures 12(c), 12(e)–12(g)). These two sedimentary samples (21T50 and 21T55) were probably sourced from either the Huaniushan arc or the Shibanshan arc.

In summary, an independent intraoceanic arc was the primary source for the Permian matrix of the Houhongquan ophiolitic mélange. The Huaniushan arc or the Shibanshan arcs were the provenances for the Triassic sandstone matrixes.

6.4. Tectonic Evolution and Implications for the Altaiids. Our geological mapping reveals that the mafic rocks are thrust-imblicated within the Houhongquan ophiolitic mélange complex. The basalts and gabbros demonstrate the N-MOR- and SSZ-type ophiolitic geochemical signatures. The chert blocks contain radiolarian and sponge ancient needles ([43], Supplement Figure 1). All the data suggest that they are the relic fragments of the ophiolite [62, 63]. In addition, zircon U–Pb ages reveal oceanic crustal blocks in the Liuyuan accretionary complex age ranging from 1071 Ma to 270 Ma, as previously described (Figure 11(a)). The sedimentary and metamorphic sedimentary blocks have the MDAs that range from 457 Ma to 222 Ma ([9, 64], this study).

In the Eastern Tianshan to Beishan orogen, no consensus regarding the closure timing of the Paleo-Asian Ocean emerged, to date, the proposed timing ranging from Devonian to Triassic. The main models proposed by different authors include (1) Devonian [10, 65], (2) Carboniferous [8, 9, 11], (3) Latest Carboniferous–Early Permian [66], (4) Late Permian [3, 16], and (5) Late Triassic [41, 67–70]. Our new geochronological results of the Houhongquan ophiolitic mélange indicate that the Liuyuan–Houhongquan Ocean was still subducting at ca. 222 Ma.

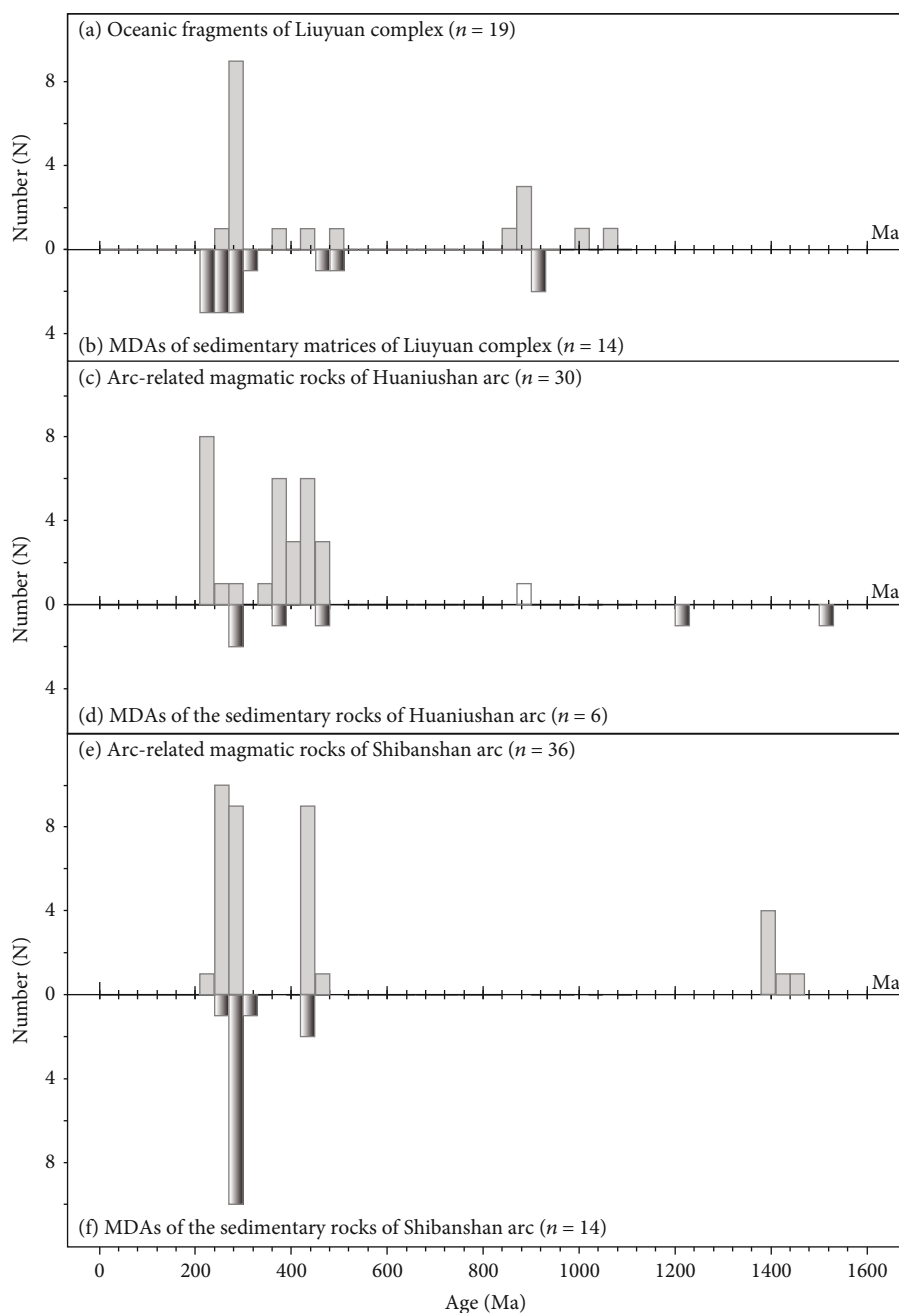


FIGURE 11: Histograms of the magmatism and sedimentary rocks of the (a, b) Liuyuan accretionary complex, (c, d) Huaniushan arc, and (e, f) Shibanshan arc. Data are after Table 2.

As discussed before, although geologists hold different viewpoints on oceanic basin type of the Liuyuan–Houhongquan Ocean during the Permian to late Triassic, their comprehensive studies also suggest that the Liuyuan–Houhongquan Ocean basin closed by the southward thrust and folded during the Late Triassic. For example, (1) Wang et al. [9] suggest that the Liuyuan rift basin closed during 230–227 Ma, (2) Tian & Xiao [34] suggest that the Liuyuan back-arc basin closed until 217 Ma, and (3) the branch of the Paleo-Asian Ocean closed posterior to the Late Triassic in the Eastern Tianshan–Beishan region [69, 71].

In recent years, some lines of evidence have reported the existence of the Paleo-Asian Ocean in the Late Triassic in the Tianshan–Beishan orogens: (1) Late Triassic (ca. 234 Ma) sedimentary matrix in the Kanguer mélangé [67]; (2) multiple sources before the Permian–Triassic, as indicated by sedimentary rocks between the Dananhu and Yamansu arcs [68]; (3) Middle to Late Triassic adakite-like, arc-related granites and mafic plutons from eastern Tianshan to Beishan orogen [9, 22, 34, 72–74]; (4) Mid–Late Triassic eclogite facies metamorphic rocks and forearc sedimentary rocks in the western Tianshan [14, 75–77]; (5)

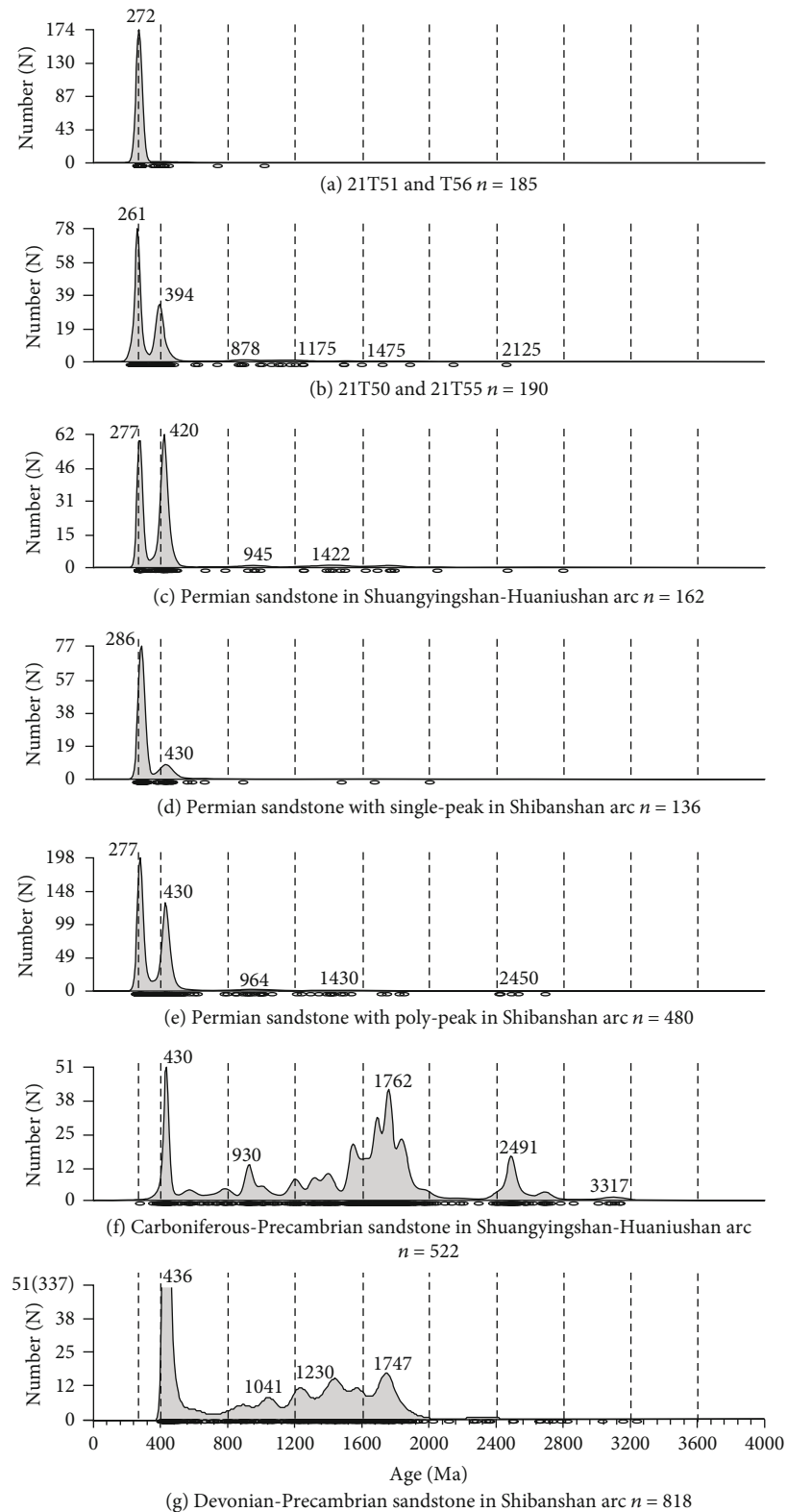


FIGURE 12: Histogram plots for the sedimentary rocks in Houhongquan ophiolitic mélangé and adjacent areas. (a, b) Four sandstones from the Houhongquan ophiolitic mélangé. (c–e) Permian sandstones in the Huaniushan arc and the Shibanshan arc. (f, g) Carboniferous–Precambrian sandstones from the Huaniushan arc and Shibanshan arc. These data suggest that an intraoceanic arc developed in the Liuyuan–Houhongquan Ocean. Data of (d) Permian sandstone in the Huaniushan arc [33]; (e) Permian sandstone with a single peak in the Shibanshan arc [33, 34]; (f) Permian sandstone with a polypeak in the Shibanshan arc [33, 38]; (g) Carboniferous–Precambrian sandstone in the Huaniushan arc [31, 33, 57]; (e) Devonian–Precambrian sandstone in the Shibanshan arc [19].

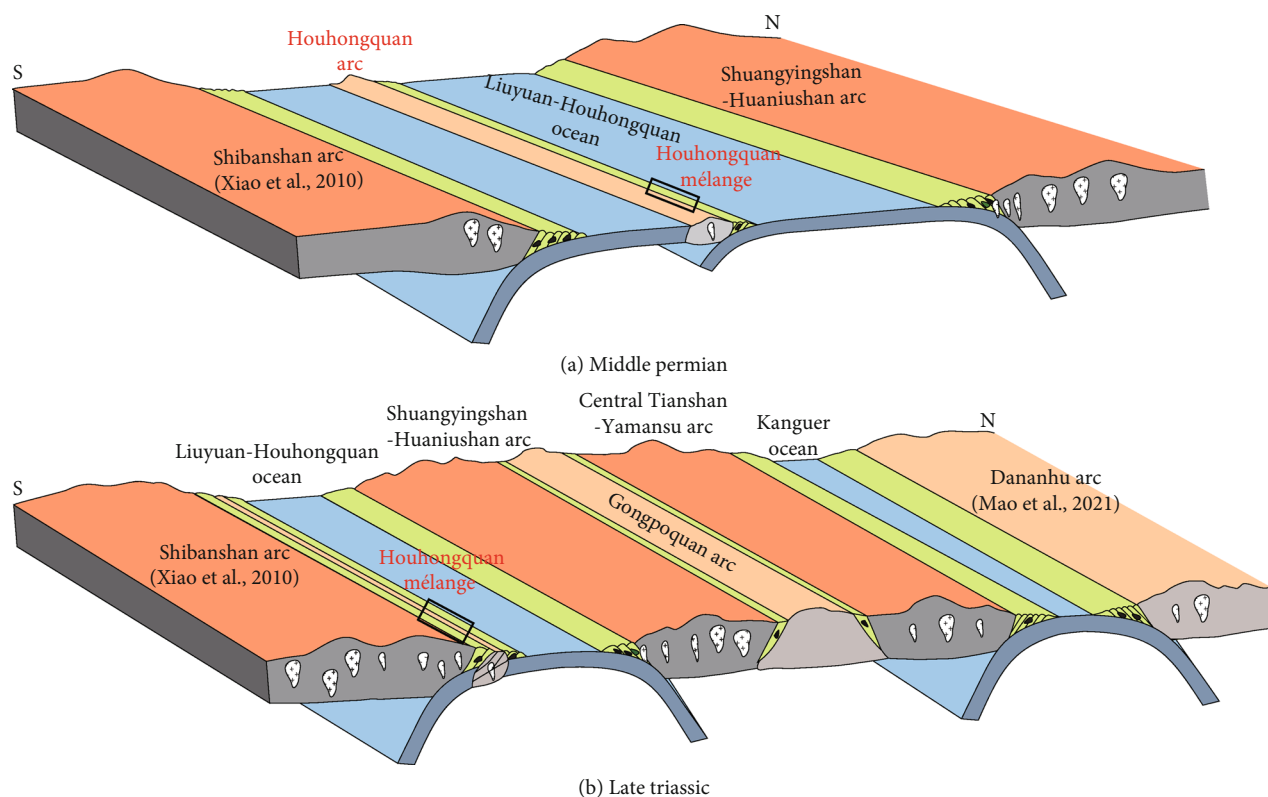


FIGURE 13: Tectonic model of the eastern Tianshan and Beishan orogen in the Permian to Triassic. (a) In the Middle Permian, the Liuyuan–Houhongquan Ocean remained open and subducted bidirectionally. The Liuyuan–Houhongquan Ocean is a multi-island ocean that developed two continental arcs and an intraoceanic arc (Houhongquan). The N-MOR and SSZ-affinity mafic rocks and cherts were tectonic emplaced into the forearc accretionary prism of the Houhongquan arc. (b) During the Late Triassic (234–222 Ma), the Houhongquan arc docked on the northern margin of the Shibanshan continental arc. The Liuyuan–Houhongquan Ocean and the Kanguer–Hongshishan Ocean were also not simultaneously closed, suggesting an archipelago setting in the southern Altai.

tectonic SN-trending thrusting and folding occurred [9, 34]; and (6) tectonic relations also support that the oceanic basins closed after ca. 232 Ma [3, 15, 69, 71]. Combined with previous data, we propose a new model for the eastern Tianshan–Beishan orogen during Permian to Triassic.

- (1) During Middle Permian, an intraoceanic arc developed in the Liuyuan–Houhongquan Ocean and deposited sandstone with Middle Permian MDAs and a single peak of detrital zircon age (Figure 13(a)). The intraoceanic subduction zone was amalgamated and welded to the Shibanshan continental arc during Middle Permian to Late Triassic and led to the emplacement of these intraoceanic arc-sourced sandstone blocks in the forearc mélangé [33, 34]
- (2) During Late Triassic, the Ocean was not closed in the eastern Tianshan and Beishan orogen (Figure 13(b)). Moreover, at least two oceanic basins of the Paleo-Asian Ocean existed, e.g., the Liuyuan–Houhongquan Ocean and the Kanguer Ocean [67, 73]

The Liuyuan–Houhongquan Ocean may be a limited narrow ocean basin in the Late Triassic because the sandstone blocks in the Houhongquan ophiolitic mélangé con-

tain a certain proportion of Precambrian zircons compared to the Permian sandstones. The Kanguer Ocean is a limited narrow ocean basin that cannot prevent material exchange from the Dananhu and Yamansu arcs [67, 68, 70]. The Liuyuan–Houhongquan Ocean subducted bidirectionally below the Huaniushan arc and the Shibanshan arc, resulting in voluminous arc-related magmatism: (1) in the Huaniushan arc, the 240–238 Ma adakite-like granites [22], the 249–234 Ma arc-related granites [72, 74], the calc–alkaline 228 Ma mafic rocks [78], and the 225–217 Ma I-type granite-related A_2 -type high-fractionation orogenic granites [22, 70]; (2) in the Shibanshan arc, the 241 Ma arc-related granite was also reported [19]. Combining with the Mid–Late Triassic eclogites and forearc sedimentary rocks in the Western Tianshan [14, 75, 77, 79], we conclude that the Tarim Craton and Dunhuang block finally docked at the Altai at the Late Triassic.

7. Conclusions

- (1) Geological mapping and field relationships indicate that the Houhongquan ophiolitic mélangé is characterized by top-to-south thrusting with block-in-matrix structure. The relics of the subducted

oceanic plate contains the blocks of gabbro, pillow basalt, massive basalt, and radiolarian cherts

- (2) The basalts and gabbros in the Houhongquan ophiolitic mélange contain N-MOR- and SSZ-type ophiolite
- (3) The MDAs of the sandstone blocks from the Houhongquan ophiolitic mélange are 222 ± 5 Ma, 233.8 ± 2.3 Ma, 263.4 ± 2.5 Ma, and 263.5 ± 2.8 Ma, respectively. These dating results indicate that the Liuyuan–Houhongquan Ocean closed at ca. 222 Ma
- (4) The sandstone blocks from the Houhongquan ophiolitic mélange display two types of detrital age patterns. The Middle Permian MDA sandstones have a single Middle Permian with a Devonian peak, indicating an intraoceanic arc. However, the Late Triassic MDA sandstones have multiple peaks and contain Precambrian zircons, suggesting that they were sourced from a continental arc. These results indicated that the Liuyuan–Houhongquan Ocean was a multi-island ocean in the Middle Permian and that the intraoceanic arc docked on the Shibanshan arc in the Late Triassic and terminated the Paleo-Asian Ocean in this part of the southern Altaids

Data Availability

The data for this study are available in this manuscript and supplementary material.

Conflicts of Interest

The authors declare that they have no conflicts of interest.

Acknowledgments

This study was financially supported by the Third Xinjiang Scientific Expedition Program (2022xjkk1301), the National Natural Science Foundation of China (41888101, 41822204), One Hundred Talent Program of the Chinese Academy of Sciences (E2250403), and Science and Technology Major Project of Xinjiang Uygur Autonomous Region, China (2021A03001 and 2022A03010-1), and Youth Innovation Promotion Association of the Chinese Academy of Sciences (2022446). This contributes to IGCP 622, IGCP 669, and IGCP 710.

Supplementary Materials

Supplementary Table 1: U–Pb ages of detrital zircons of sedimentary rocks and granite from the Houhongquan ophiolitic mélange. Highly discordant analyses (con.% < 90% or > 110%) are considered unusable and displayed in strike-through text and not included in the concordia diagrams. $\text{Concord}\% = 100 * ({}^{207}\text{Pb}/{}^{206}\text{Pb}) \text{ age} / ({}^{206}\text{Pb}/{}^{238}\text{U}) \text{ age}$ for age > 1500 Ma or $100 * ({}^{207}\text{Pb}/{}^{235}\text{U}) \text{ age} / ({}^{206}\text{Pb}/{}^{238}\text{U}) \text{ age}$ for age < 1500 Ma. Supplementary Table 2: the regional age data for the Houhongquan ophiolitic mélange in southern Beishan orogen. Supplementary Figure 1: the photographs of the radiolarians in the cherts of the Houhongquan ophiolitic mélange. Supplementary Figure 2: binary diagrams illustrating SiO₂ vs. major and trace elements of the basalt and gabbro in the Houhongquan ophiolitic mélange. Supplementary Analytical methods. (*Supplementary Materials*)

Supplementary Figure 2: binary diagrams illustrating SiO₂ vs. major and trace elements of the basalt and gabbro in the Houhongquan ophiolitic mélange. Supplementary Analytical methods. (*Supplementary Materials*)

References

- [1] K. Schulmann and S. Paterson, “Asian continental growth,” *Nature Geoscience*, vol. 4, no. 12, pp. 827–829, 2011.
- [2] A. M. C. Şengör, B. A. Natal’in, and U. S. Burtman, “Evolution of the Altaid tectonic collage and Paleozoic crustal growth in Eurasia,” *Nature*, vol. 364, pp. 209–304, 1993.
- [3] W. J. Xiao, B. F. Windley, C. M. Han et al., “Late Paleozoic to early Triassic multiple roll-back and oroclinal bending of the Mongolia collage in Central Asia,” *Earth-Science Reviews*, vol. 186, pp. 94–128, 2018.
- [4] N. L. Dobretsov, N. A. Berzin, and M. M. Buslov, “Opening and the tectonic evolution of Paleo-Asian ocean,” *International Geology Review*, vol. 35, pp. 335–360, 1995.
- [5] A. Kröner, B. F. Windley, G. Badarch et al., “Accretionary growth and crust formation in the Central Asian Orogenic Belt and comparison with the Arabian-Nubian shield,” *Geological Society of America Memoirs*, vol. 200, pp. 181–209, 2007.
- [6] B. F. Windley, D. Alexeiev, W. Xiao, A. Kröner, and G. Badarch, “Tectonic models for accretion of the Central Asian Orogenic Belt,” *Journal of the Geological Society, London*, vol. 164, no. 1, pp. 31–47, 2007.
- [7] J. Gao and R. Klemm, “Formation of HP-LT rocks and their tectonic implications in the western Tianshan Orogen, NW China: geochemical and age constraints,” *Lithos*, vol. 66, no. 1–2, pp. 1–22, 2003.
- [8] F. J. Nie, S. H. Jiang, D. M. Bai et al., *Metallogenic Studies and Ore Prospecting in the Conjunction Area of Inner Mongolia Autonomous Region, Gansu Province and Xinjiang Uygur Autonomous Region (Beishan Mt.), Northwest China*, Geological Publishing House, Beijing, China, 2002.
- [9] Y. Wang, Z. Luo, M. Santosh, S. Wang, and N. Wang, “The Liuyuan Volcanic Belt in NW China revisited: evidence for Permian rifting associated with the assembly of continental blocks in the Central Asian Orogenic Belt,” *Geological Magazine*, vol. 154, pp. 265–285, 2016.
- [10] Y. Yuan, K. Zong, P. A. Cawood, H. Cheng, and M. Li, “Implication of Mesoproterozoic (~1.4 Ga) magmatism within microcontinents along the southern Central Asian Orogenic Belt,” *Precambrian Research*, vol. 327, pp. 314–326, 2019.
- [11] G. C. Zuo, S. L. Zhang, G. Q. He, and Y. Zhang, “Plate tectonic characteristics during the early Paleozoic in Beishan near the Sino-Mongolian border region, China,” *Tectonophysics*, vol. 188, no. 3–4, pp. 385–392, 1991.
- [12] B. Huang, D. Fu, T. Kusky, K. Ruan, W. Zhou, and X. Zhang, “Sedimentary provenance in response to Carboniferous arc-basin evolution of East Junggar and North Tianshan belts in the southwestern Central Asian Orogenic Belt,” *Tectonophysics*, vol. 722, pp. 324–341, 2018.
- [13] Q. G. Mao, W. J. Xiao, B. F. Windley et al., “The Liuyuan complex in the Beishan, NW China: a Carboniferous-Permian ophiolitic fore-arc sliver in the southern Altaids,” *Geological Magazine*, vol. 149, no. 3, pp. 483–506, 2012.
- [14] Z. Tan, W. Xiao, Q. Mao et al., “Final closure of the Paleo-Asian Ocean basin in the early Triassic,” *Communications Earth & Environment*, vol. 3, no. 1, p. 259, 2022.

- [15] K. Wang, W. Xiao, B. F. Windley et al., “The Dashui subduction complex in the eastern Tianshan-Beishan Orogen (NW China): long-lasting subduction-accretion terminated by unique mid-Triassic strike-slip juxtaposition of arcs in the southern Altaids,” *Tectonics*, vol. 41, no. 6, p. e2021TC007190, 2022.
- [16] W. J. Xiao, Q. G. Mao, B. F. Windley et al., “Paleozoic multiple accretionary and collisional processes of the Beishan orogenic collage,” *American Journal of Science*, vol. 310, no. 10, pp. 1553–1594, 2010.
- [17] X. Y. Liu and Q. Wang, “Tectonics of orogenic belts in the Beishan Mountains, western China and their evolution,” *Geoscience Studies*, vol. 28, pp. 37–48, 1995.
- [18] Q. Mao, W. Xiao, T. Fang et al., “Late Ordovician to early Devonian adakites and Nb-enriched basalts in the Liuyuan area, Beishan, NW China: implications for early Paleozoic slab-melting and crustal growth in the southern Altaids,” *Gondwana Research*, vol. 22, no. 2, pp. 534–553, 2012.
- [19] R. Zheng, J. Li, J. Zhang, and W. Xiao, “A prolonged subduction-accretion in the southern Central Asian Orogenic Belt: insights from anatomy and tectonic affinity for the Beishan complex,” *Gondwana Research*, vol. 95, pp. 88–112, 2021.
- [20] Z. Y. He, R. Klemd, L. L. Yan, and Z. M. Zhang, “The origin and crustal evolution of microcontinents in the Beishan orogen of the southern Central Asian Orogenic Belt,” *Earth-Science Reviews*, vol. 185, pp. 1–14, 2018.
- [21] W. M. Saktura, S. Buckman, A. P. Nutman, E. Belousova, Z. Yan, and J. C. Aitchison, “Continental origin of the Gubaoquan eclogite and implications for evolution of the Beishan Orogen, Central Asian Orogenic Belt, NW China,” *Lithos*, vol. 294–295, pp. 20–38, 2017.
- [22] S. Li, T. Wang, S. A. Wilde, Y. Tong, D. Hong, and Q. Guo, “Geochronology, petrogenesis and tectonic implications of Triassic granitoids from Beishan, NW China,” *Lithos*, vol. 134–135, pp. 123–145, 2012.
- [23] L. A. Raymond, “Perspectives on the roles of melanges in subduction accretionary complexes: a review,” *Gondwana Research*, vol. 74, pp. 68–89, 2019.
- [24] C. Benyon, A. Leier, D. A. Leckie, A. Webb, S. M. Hubbard, and G. Gehrels, “Provenance of the Cretaceous Athabasca Oil Sands, Canada: implications for continental-scale sediment transport,” *Journal of Sedimentary Research*, vol. 84, no. 2, pp. 136–143, 2014.
- [25] W. A. Matthews, B. Guest, D. Coutts, H. Bain, and S. Hubbard, “Detrital zircons from the Nanaimo basin, Vancouver Island, British Columbia: an independent test of Late Cretaceous to Cenozoic northward translation,” *Tectonics*, vol. 36, no. 5, pp. 854–876, 2017.
- [26] P. A. Cawood, C. J. Hawkesworth, and B. Dhuime, “Detrital zircon record and tectonic setting,” *Geology*, vol. 40, no. 10, pp. 875–878, 2012.
- [27] D. S. Coutts, W. A. Matthews, and S. M. Hubbard, “Assessment of widely used methods to derive depositional ages from detrital zircon populations,” *Geoscience Frontiers*, vol. 10, no. 4, pp. 1421–1435, 2019.
- [28] C. M. Fedo, K. N. Sircombe, and R. H. Rainbird, “Detrital zircon analysis of the sedimentary record,” *Reviews in Mineralogy and Geochemistry*, vol. 53, no. 1, pp. 277–303, 2003.
- [29] D. R. Nelson, “An assessment of the determination of depositional ages for precambrian clastic sedimentary rocks by U-Pb dating of detrital zircons,” *Sedimentary Geology*, vol. 141–142, pp. 37–60, 2001.
- [30] Q. Q. Guo, W. J. Xiao, Q. L. Hou et al., “Construction of Late Devonian Dundunshan arc in the Beishan orogen and its implication for tectonics of southern Central Asian Orogenic Belt,” *Lithos*, vol. 184–187, pp. 361–378, 2014.
- [31] D. Song, W. Xiao, C. Han, Z. Tian, and Z. Wang, “Provenance of metasedimentary rocks from the Beishan orogenic collage, southern Altaids: constraints from detrital zircon U-Pb and Hf isotopic data,” *Gondwana Research*, vol. 24, no. 3–4, pp. 1127–1151, 2013.
- [32] GSBGMR, *Regional Geology of Gansu Province, Geological Memoirs*, Geological Publishing House, Beijing, China, 1989.
- [33] Q. Liu, G. Zhao, Y. Han et al., “Detrital zircon provenance constraints on the final closure of the middle segment of the Paleo-Asian Ocean,” *Gondwana Research*, vol. 69, pp. 73–88, 2019.
- [34] Z. Tian and W. Xiao, “An Andean-type arc transferred into a Japanese-type arc at final closure stage of the Palaeo-Asian Ocean in the southernmost of Altaids,” *Geological Journal*, vol. 55, no. 3, pp. 2023–2043, 2020.
- [35] Z. H. Zhao, Z. J. Guo, and Y. Wang, “Geochronology, geochemical characteristics and tectonic implications of the granitoids from Liuyuan area, Beishan, Gansu province, northwest China,” *Acta Petrologica Sinica*, vol. 23, pp. 1847–1860, 2007.
- [36] J. Duan, G. Xu, Z. Z. Qian et al., “Petrogenesis and Ni-Cu exploration potential of Devonian mafic-ultramafic intrusions in the southern part of the Central Asian Orogenic Belt, NW China: Constraints from zircon O isotopes and whole-rock Sr-Nd isotopes,” *International Geology Review*, vol. 64, no. 11, pp. 1495–1513, 2022.
- [37] W. Xie, X. Y. Song, Y. F. Deng et al., “Geochemistry and petrogenetic implications of a Late Devonian mafic-ultramafic intrusion at the southern margin of the Central Asian Orogenic Belt,” *Lithos*, vol. 144–145, pp. 209–230, 2012.
- [38] D. Song, W. Xiao, B. F. Windley, C. Han, and Y. Lei, “Metamorphic complexes in accretionary orogens: insights from the Beishan collage, southern Central Asian Orogenic Belt,” *Tectonophysics*, vol. 688, pp. 135–147, 2016.
- [39] Y. Yuan, K. Zong, Z. He et al., “Geochemical and geochronological evidence for a former early Neoproterozoic microcontinent in the South Beishan Orogenic Belt, southernmost Central Asian Orogenic Belt,” *Precambrian Research*, vol. 266, pp. 409–424, 2015.
- [40] W. Zhang, T. R. Wu, Y. K. He, J. C. Feng, and R. G. Zheng, “LA-ICP-MS zircon U–Pb ages of Xijian quanzi alkali-rich potassium-high granites in Beishan, Gansu Province, and their tectonic significances,” *Acta Petrology Mineral*, vol. 29, pp. 719–731, 2010.
- [41] R. Zheng, J. Li, J. Zhang, W. Xiao, and Q. Wang, “Permian oceanic slab subduction in the southmost of Central Asian Orogenic Belt: evidence from adakite and high-Mg diorite in the southern Beishan,” *Lithos*, vol. 358–359, article 105406, 2020.
- [42] J. Y. Yu, X. G. Li, G. Q. Wang, P. Wu, and Q. J. Yan, “Zircon U-Pb ages of Huitongshan and Zhangfangshan ophiolite in Beishan of Gansu-Inner Mongolia border area and their significance,” *Geological Bulletin of China*, vol. 31, pp. 2038–2045, 2012.
- [43] J. Shi, J. Lu, J. Wei et al., “Petrology, geochemistry and sedimentary environment of Permian siliceous rocks in Yinggen-Ejin basin and its adjacent areas,” *Geological Bulletin of China*, vol. 37, pp. 120–131, 2018.

- [44] R. Zheng, T. Wu, Z. Wen, Q. Meng, and Z. Zhang, "Geochronology and geochemistry of late Paleozoic magmatic rocks in the Yinwaxia area, Beishan: implications for rift magmatism in the southern Central Asian Orogenic Belt," *Journal of Asian Earth Sciences*, vol. 91, pp. 39–55, 2014.
- [45] X. Guo, S. Chen, R. Gou, X. Liu, Q. Wang, and Q. Pu, "The geochemistry, ageological characteristics and causes of marine basalts in Houhongquan area, Beishan," *Gansu and Inner Mongolia. Earth Science*, vol. 46, no. 11, pp. 3945–3964, 2021.
- [46] C. Y. Jiang, M. Z. Xia, X. Yu, D. X. Lu, W. Wei, and S. F. Ye, "Liuyuan trachybasalt belt in the northeastern Tarim plate: products of asthenosphere mantle decompressional melting," *Acta Petrologica Sinica*, vol. 23, pp. 1765–1778, 2007.
- [47] W. V. Boynton, "Geochemistry of the rare earth elements: meteorite study," in *Rare Earth Element Geochemistry: Elsevier*, P. Henderson, Ed., pp. 63–114, Amsterdam, UK, 1984.
- [48] S. S. Sun and W. F. McDonough, "Chemical and isotopic systematic of oceanic basalts: implications for mantle composition and process," in *Magmatism in the Ocean Basins*, A. D. Sowers and M. J. Norry, Eds., pp. 313–345, Geological Society Special Publication, 1989.
- [49] S. R. Hart and H. Staudigel, "The control of alkalis and uranium in seawater by ocean crust alteration," *Earth and Planetary Science Letters*, vol. 58, no. 2, pp. 202–212, 1982.
- [50] W. Xu, X. Xu, Y. Niu et al., "Geochronology and petrogenesis of the Permian marine basalt in the southern Beishan region and their tectonic implications," *Acta Geologica Sinica*, vol. 93, pp. 1928–1953, 2019.
- [51] Y. Dilek and H. Furnes, "Ophiolite genesis and global tectonics: geochemical and tectonic fingerprinting of ancient oceanic lithosphere," *Geological Society of America Bulletin*, vol. 123, no. 3-4, pp. 387–411, 2011.
- [52] J. A. Pearce, "Geochemical fingerprinting of oceanic basalts with applications to ophiolite classification and the search for Archean oceanic crust," *Lithos*, vol. 100, no. 1-4, pp. 14–48, 2008.
- [53] J. W. Shervais, "Ti-V plots and the petrogenesis of modern and ophiolitic lavas," *Earth and Planetary Science Letters*, vol. 59, no. 1, pp. 101–118, 1982.
- [54] D. A. Wood, "The application of a ThHfTa diagram to problems of tectonomagmatic classification and to establishing the nature of crustal contamination of basaltic lavas of the British Tertiary Volcanic Province," *Earth and Planetary Science Letters*, vol. 50, no. 1, pp. 11–30, 1980.
- [55] Y. Z. Niu, J. C. Lu, C. Y. Liu, B. Song, J. Z. Shi, and W. Xu, "Chronostratigraphy of marine Permian in the Beishan region, north China and its correlation," *Acta Geologica Sinica*, vol. 92, pp. 1131–1148, 2018.
- [56] P. A. Floyd and B. E. Leveridge, "Tectonic environment of the Devonian Gramscatho basin, south Cornwall: framework mode and geochemical evidence from turbiditic sandstones," *Journal of the Geological Society*, vol. 144, no. 4, pp. 531–542, 1987.
- [57] S. Ao, W. Xiao, B. F. Windley et al., "Paleozoic accretionary orogenesis in the eastern Beishan orogen: Constraints from zircon U-Pb and $^{40}\text{Ar}/^{39}\text{Ar}$ geochronology," *Gondwana Research*, vol. 30, pp. 224–235, 2016.
- [58] I. Safonova, A. Perfilova, O. Obut et al., "Traces of intra-oceanic arcs recorded in sandstones of eastern Kazakhstan: implications from U-Pb detrital zircon ages, geochemistry, and Nd-Hf isotopes," *International Journal of Earth Sciences*, vol. 111, no. 8, pp. 2449–2468, 2022.
- [59] M. Rioux, B. Hacker, J. Mattinson, P. Kelemen, J. Blusztajn, and G. Gehrels, "Magmatic development of an intra-oceanic arc: high-precision U-Pb zircon and whole-rock isotopic analyses from the accreted Talkeetna arc, south-central Alaska," *Geological Society of America Bulletin*, vol. 119, no. 9-10, pp. 1168–1184, 2007.
- [60] D. Cluzel and S. Meffre, "In search of Gondwana heritage in the Outer Melanesian Arc: no pre-upper Eocene detrital zircons in Viti Levu river sands (Fiji Islands)," *Australian Journal of Earth Sciences*, vol. 66, no. 2, pp. 265–277, 2019.
- [61] A. K. Schmitt, K. Konrad, G. D. Andrews et al., " $^{40}\text{Ar}/^{39}\text{Ar}$ ages and zircon petrochronology for the rear arc of the Izu-Bonin-Marianas intra-oceanic subduction zone," *International Geology Review*, vol. 60, no. 8, pp. 956–976, 2018.
- [62] Y. Isozaki, S. Maruyama, and F. Furuoka, "Accreted oceanic materials in Japan," *Tectonophysics*, vol. 181, no. 1-4, pp. 179–205, 1990.
- [63] T. M. Kusky, B. F. Windley, I. Safonova et al., "Recognition of ocean plate stratigraphy in accretionary orogens through Earth history: a record of 3.8 billion years of sea floor spreading, subduction, and accretion," *Gondwana Research*, vol. 24, no. 2, pp. 501–547, 2013.
- [64] Q. Mao, W. Xiao, H. Wang et al., "Prolonged late Mesoproterozoic to late Triassic tectonic evolution of the major Paleo-Asian Ocean in the Beishan orogen (NW China) in the southern Altai," *Frontiers in Earth Science*, vol. 9, 2022.
- [65] L. Q. Xia, X. Y. Xu, Z. C. Xia, X. M. Li, Z. P. Ma, and L. S. Wang, "Petrogenesis of Carboniferous rift-related volcanic rocks in the Tianshan, northwestern China," *Geological Society of America Bulletin*, vol. 116, no. 3, pp. 419–433, 2004.
- [66] W. J. Xiao, L. C. Zhang, K. Z. Qin, S. Sun, and J. L. Li, "Paleozoic accretionary and collisional tectonics of the Eastern Tianshan (China): Implications for the continental growth of central Asia," *American Journal of Science*, vol. 304, no. 4, pp. 370–395, 2004.
- [67] S. J. Ao, Q. G. Mao, B. F. Windley et al., "The youngest matrix of 234 Ma of the Kanguer accretionary mélange containing blocks of N-MORB basalts: constraints on the northward subduction of the Paleo-Asian Kanguer Ocean in the Eastern Tianshan of the southern Altai," *International Journal of Earth Science*, vol. 110, no. 3, pp. 791–808, 2021.
- [68] Z. Chen, W. Xiao, B. F. Windley et al., "Composition, provenance, and tectonic setting of the southern Kanguer accretionary complex in the eastern Tianshan, NW China: implications for the late Paleozoic evolution of the north Tianshan Ocean," *Tectonics*, vol. 38, no. 8, pp. 2779–2802, 2019.
- [69] M. Domeier and T. H. Torsvik, "Plate tectonics in the late Paleozoic," *Geoscience Frontiers*, vol. 5, no. 3, pp. 303–350, 2014.
- [70] Q. G. Mao, S. J. Ao, B. F. Windley, J. B. Wang, Y. C. Li, and W. J. Xiao, "Middle Triassic lower crust-derived adakitic magmatism: thickening of the Dananhu intra-oceanic arc and its implications for arc-arc amalgamation in the Eastern Tianshan (NW China)," *Geological Journal*, vol. 56, no. 6, pp. 3137–3154, 2021.
- [71] C. Wilhem, B. F. Windley, and G. M. Stampfli, "The Altai of Central Asia: A tectonic and evolutionary innovative review," *Earth-Science Reviews*, vol. 113, no. 3-4, pp. 303–341, 2012.

- [72] L. Guo, G. Wang, L. Guo, and T. Bu, "Petrogenesis of Early Triassic felsic dikes in the Lucaogou area of southern Beishan orogenic belt," *Bulletin of Mineralogy, Petrology and Geochemistry*, vol. 37, pp. 502–512, 2018.
- [73] Q. G. Mao, S. J. Ao, B. F. Windley et al., "Middle-Late Triassic southward-younging granitoids: tectonic transition from subduction to collision in the Eastern Tianshan-Beishan Orogen (NW China)," *Geological Society of America Bulletin*, vol. 134, no. 9-10, pp. 2206–2224, 2022.
- [74] Z. Yang, J. Zhao, D. Jiang, Q. Zhao, J. Zhang, and X. Fang, "Chronological and geochemical characteristics of the porphyritic granodiorite in the Qiahongquan area, Beishan region, Gansu province, China and their tectonic significances," *Bulletin of Mineralogy, Petrology and Geochemistry*, vol. 2021, pp. 228–241, 2021.
- [75] M. Sang, W. Xiao, A. Bakirov, R. Orozbaev, K. Sakiev, and K. Zhou, "Oblique wedge extrusion of UHP/HP complexes in the Late Triassic: structural analysis and zircon ages of the Atbashi Complex, South Tianshan, Kyrgyzstan," *International Geology Review*, vol. 59, no. 10, pp. 1369–1389, 2017.
- [76] M. Sang, W. J. Xiao, R. Orozbaev et al., "Structural styles and zircon ages of the South Tianshan accretionary complex, Atbashi Ridge, Kyrgyzstan: insights for the anatomy of ocean plate stratigraphy and accretionary processes," *Journal of Asian Earth Sciences*, vol. 153, pp. 9–41, 2018.
- [77] L. Zhang, Y. Ai, X. Li et al., "Triassic collision of western Tianshan orogenic belt, China: evidence from SHRIMP U-Pb dating of zircon from HP/UHP eclogitic rocks," *Lithos*, vol. 96, no. 1-2, pp. 266–280, 2007.
- [78] H. R. Sun, Z. C. Lü, X. F. Yu et al., "Early Mesozoic tectonic evolution of Beishan orogenic belt: constraints from chronology and geochemistry of the late Triassic diabase dyke in Liuyuan area, Gansu province," *Acta Petrologica Sinica*, vol. 36, pp. 1755–1768, 2020.
- [79] M. Sang, W. Xiao, and B. F. Windley, "Unravelling a Devonian–Triassic seamount chain in the South Tianshan high-pressure/ultrahigh-pressure accretionary complex in the Atbashi area (Kyrgyzstan)," *Geological Journal*, vol. 55, no. 3, pp. 2300–2317, 2020.
- [80] J. A. Winchester and P. A. Floyd, "Geochemical discrimination of different magma series and their differentiation products using immobile elements," *Chemical Geology*, vol. 20, pp. 325–343, 1977.
- [81] A. Myashiro, "Volcanic rock series in island arcs and active continental margins," *American Journal of Science*, vol. 274, no. 4, pp. 321–355, 1974.
- [82] A. Zindler and S. R. Hart, "Chemical geodynamics," *Annual Reviews of Earth and Planetary Sciences*, vol. 14, no. 1, pp. 493–571, 1986.
- [83] J. W. Hawkins, "Geology of supra-subduction zones—implications for the origin of ophiolites," *Geological Society of America Special Paper*, vol. 373, pp. 227–268, 2003.